Long-term high temperatures affect seed maturation and seed coat integrity in *Brassica napus*

Unnikannan Prabhullachandran[1, 2], Ivana Urbánková[3], Alejandro Medaglia-Mata[4,5], Audrey Creff[6], Aline Voxeur[7], Ivan Petřík[8], Aleš Pěnčík[8], Ondřej Novák[8], Benoit Landrein[6], Jan Hejátko[3], Hélène S. Robert[1]

1. Hormonal Crosstalk in Plant Development, Mendel Center for Plant Genomics and Proteomics, Central European Institute of Technology (CEITEC), Masaryk University, Brno, Czech Republic

2. Laboratory of Functional Genomics and Proteomics, National Centre for Biomolecular Research, Faculty of Science, Masaryk University, Brno, Czech Republic

3. Functional Genomics and Proteomics of Plants, Mendel Center for Plant Genomics and Proteomics, Central European Institute of Technology (CEITEC), Masaryk University, Brno, Czech Republic

4. Bioinformatics Core Facility, Central European Institute of Technology (CEITEC), Masaryk University, Brno, Czech Republic

5. Department of Biology, Faculty of Medicine, Masaryk University, Brno, Czech Republic

6. Laboratoire Reproduction et Développement des Plantes, Université de Lyon, ENS de Lyon, UCB Lyon, CNRS, INRAE, INRIA, Lyon, France

7. Université Paris-Saclay, INRAE, AgroParisTech, Institute Jean-Pierre Bourgin for Plant Science (IJPB), Versailles, France

8. Laboratory of Growth Regulators, Faculty of Science, Palacký University and Institute of Experimental Botany, The Czech Academy of Sciences, Olomouc, Czech Republic

Hélène S. Robert (corresponding author helene.robert.boisivon@ceitec.muni.cz)

ORCID

UK 0000-0001-6430-575X

AMM 0000-0003-3496-0571

AC 0000-0001-7736-5882

AV 0000-0001-9452-6756

IP 0000-0001-5320-7599

AP 0000-0002-1314-2249

ON 0000-0003-3452-0154
BL 0000-0002-2371-9996
JH 0000-0002-2622-6046
HSR 0000-0002-6610-836X

Word count 7837
Number of Figures 6
Supporting Information Method S1**,** Figures S1-S6 and Tables S1-S4

SUMMARY

- Temperatures above the optimum growth temperature affect seed development, producing seeds with ruptured seed coats. This phenotype is associated with accelerated embryo development. However, the molecular mechanism underlying this effect remains unclear.
- To investigate the occurrence of temperature-induced seed coat rupture, we combined detailed phenotyping approaches of oilseed rape seeds with transcriptomics, histology, immunolabelling, hormone and cell wall profiling.
- Our data suggest that high temperatures accelerate embryo growth, resulting in the formation of larger embryos but not larger seeds. The formation of large embryos increased the mechanical pressure exerted by the embryo on the seed coat cells, reducing their thickness. The seed coat began to mature prematurely with the accumulation of demethylesterified pectin, possibly making the cell wall stiffer. Application of abscisic acid, a hormone involved in seed dormancy, did not rescue the seed coat rupture phenotype. Hormonal and transcriptional profiling indicated that the embryo did not enter dormancy.
- Prolonged high temperatures during seed development accelerated embryo growth by stimulating cell division, while the seed coat, which depends on cell elongation, could not withstand the tension exerted by the embryo, started seed maturation and eventually ruptured.

KEYWORDS

Brassica napus, cell wall, long-term high temperature, pectin, seed coat rupture, seed development

INTRODUCTION

The adverse impacts of global warming on agricultural production pose a major challenge to global food security in the 21st century. Extreme weather events, such as heat stress, drought and floods, have been observed to reduce crop yields and shorten growing seasons, particularly in warm tropical regions. This has the potential to affect the production of staple crops, such as rice, wheat, maize, and soybean (Zhao *et al.*, 2017; Agnolucci & De Lipsis, 2020; Jägermeyr *et al.*, 2021; Heino *et al.*, 2023). The mean global temperature increase in 2023 was 1.36°C above preindustrial levels (National Aeronautics and Space Administration, 2024), highlighting the need to adapt agricultural practices to higher temperatures.

Brassica napus (canola or oilseed rape), an allotetraploid species in the Brassicaceae family, is the second most widely cultivated oilseed crop, used for the production of vegetable oil, biofuel, and protein in animal feed. Cultivation of oilseed rape at temperatures above the optimum growth temperature of 21°C for prolonged periods, especially during the flowering stage, resulted in several adverse effects, including rapid vegetative growth, reduced viability of female gametophytes, increased seed abortion rate, accelerated embryo development, and a reduction in seed oil composition (Young *et al.*, 2004; Mácová *et al.*, 2022; Secchi *et al.*, 2023). One of the distinctive phenotypes observed during seed development of certain canola cultivars subjected to prolonged heat stress that affects seed yield is the occurrence of the preharvest sprouting phenotype (PHS) (Mácová *et al.*, 2022). Misregulation of seed dormancy by abscisic acid and dormancy-related genes is considered to be the main cause of PHS in many cereal crops (Benech-Arnold & Rodríguez, 2018; Tai *et al.*, 2021). This phenotype is associated with seed coat rupture (SCR), which is observed in seeds during the early stages of maturation. The exact molecular mechanism by which this phenotype is produced at elevated temperatures remains unclear.

In Brassicaceae, seed size is regulated by the interaction between maternal and zygotic signals that coordinate the proper development of the seed coat, endosperm, and embryo (Li *et al.*, 2019). During the maturation of *Arabidopsis* seeds, the pressure generated by the interaction between the developing embryo and the endosperm within the seed, driven by embryo growth, exerts tension on the developing integuments (Creff *et al.*, 2015, 2023). The tension

generated by zygotic tissues is sensed by a specific layer of the seed coat's outer integument, the adaxial epidermis (oi1). This mechanical stimulus triggers a transcriptional response marked by the activation of the mechanosensitive gene *EUI-like P450A1* (*ELA1)*, which is believed to promote cell wall stiffening through demethylesterified pectin accumulation regulating seed size (Creff *et al.*, 2023). The dry mass of the primary plant cell wall is composed of cellulose, hemicellulose, and pectin (Cosgrove, 2024). Pectin forms a hydrated gel-like matrix in which cellulose and hemicellulose cross-link to form the cell wall. It is abundant in the middle lamella, an adhesive layer between adjacent cells. The most abundant pectin, homogalacturonan (HG), is produced in a methylesterified state, which can be demethylesterified by the activity of pectin methylesterase (PME) (Turbant *et al.*, 2016; Wu *et al.*, 2018). Blockwise removal of methyl groups can lead to the formation of Ca^{2+} cross-links, which increase the wall stiffness and inhibit growth. Alternatively, random removal can lead to pectin degradation, affecting wall rheology (Wu *et al.*, 2018).

Seed size correlates with endosperm proliferation and development. The two processes are linked by a brassinosteroid-induced cell expansion and increased levels of methylesterified pectin in the seed coat, which helps to regulate seed size (Lima *et al.*, 2024). Mechanical constriction of seed size, which restricts embryo growth, triggers the maturation programme by increasing lipid and protein storage and inhibiting embryonic cell divisions (Rolletschek *et al.*, 2021, 2024). In this study, we used a multi-method approach to investigate the occurrence of the temperature-induced SCR phenotype. The results show that SCR occurs in seeds around 20 days after pollination (20 DAP) when plants are cultivated at elevated temperatures for a prolonged period. The pressure induced by unrestricted embryo growth led to increased tension in the seed coat, characterised by reduced thickness of the seed coat layers, and resulted in early changes in cell wall composition. Accumulation of demethylesterified pectin may stiffen the cell wall of the seed coat, which may break despite being stiffened or may promote pectin degradation making the seed coat more breakable. The precise mechanism by which accelerated embryo development influences heat stress-mediated seed development in oilseed rape plants remains to be elucidated. A deeper understanding of the effects of prolonged elevated temperatures on seed development could prove invaluable in the generation of thermotolerant varieties of canola varieties, which would help to improve crop yields in the context of global warming in the 21st century.

MATERIALS AND METHODS

Plant materials and growth conditions

Two *Brassica napus* spring cultivars, Topas DH4079 and Westar, were used for this study. Seeds were sterilised, germinated, and grown initially in the phytotron (21°C, 16/8 h long day period, 150 µmol/m^2/s) until the emergence of the first flowering buds, as previously mentioned (Mácová *et al.*, 2022). Plants are then transferred to greenhouse chambers with control temperature treatment (CT) and heat treatment (HT) conditions maintained under a long-day regime (16 h light/8 h dark), LED lights with a light intensity of 150 µmol/m^2/s, 35%–45% humidity, 18°C during the night and 21°C (CT) and 32°C (HT) during the day. Seeds used for the experiments are obtained from hand-pollinated flowers. The age of the seeds is counted from the day after pollination (DAP).

Seed phenotyping

Ten hand-pollinated and dried siliques from eight plants in three biological replicates from CT and HT conditions were screened for the total, viable, dead seeds and seeds undergoing SCR (seed coat rupture with radicle or cotyledon protrusion). Fresh seeds from 14 DAP to 20 DAP were collected from Topas and Westar growing at CT and HT for embryo staging. The whole seed and its isolated embryo were imaged using a Levenhuk M500 base digital camera attached to a Zeiss stemi 305 stereomicroscope. Images were used to measure the seed and embryo areas using ImageJ from 14, 18, and 20 DAP from both conditions. The ratio of the embryo-to-seed area was calculated to get information on the space occupied by the embryo within the seed at each stage of development. Statistical significance was accounted for by a two-way ANOVA test with Sidak's multiple comparisons (* $p < 0.05$, ** $p < 0.005$, *** $p < 0.0005$, and **** $p < 0.00005$).

Hormonal measurements

Two experiments were performed. First, the hormone profiling was done on 14, 20, 26, and 36 DAP whole seeds collected from CT or HT in five replicates, each pooled from three plants. The 20, 26, and 36 DAP seeds collected from HT showing an SCR phenotype were separately collected and analysed. A second experiment was carried out on isolated embryos and seed coats of 14 and 18 DAP seeds collected from CT or HT in four replicates, each pooled from three plants. Abscisates, auxins (except indole-3-pyruvic acid; IPyA), and gibberellins were

159 determined using ultra-high-performance liquid chromatograph I-Class (Waters, Milford, CT,
160 USA) coupled with tandem mass spectrometer Xevo TQ-XS (Waters, Manchester, UK)
161 according to the "hormonomics" methodology (Šimura *et al.*, 2018). Approximately 10 mg of
162 fresh weight of each sample was aliquoted into microtubes. One ml of 60% aqueous
163 acetonitrile (v/v), a mixture of stabile isotopic labelled internal standards, and four ceramic
164 extraction beads were added into the tube. The samples were shaken in a Retsch MM400
165 oscillation mill (Haan, Germany) at 27 Hz for 5 min, sonicated for 3 min, and incubated for 30
166 min in a refrigerator. Allegra 64R benchtop centrifuge (Beckman Coulter, USA) at 20,000 rpm
167 for 15 minutes was used to separate the pellet from the supernatant. The supernatant was
168 loaded onto Oasis® HLB 30 mg/1 cc extraction cartridge (Waters, Milford, CT, USA) previously
169 activated with 1 ml methanol, water, and 60% aqueous acetonitrile (v/v). The cartridge was
170 finally washed with 60% aqueous acetonitrile (v/v). The flow-through and wash fractions were
171 collected into borosilicate glass tubes (Thermo Fisher Scientific, USA). The samples were
172 evaporated in a SpeedVac concentrator (RC1010 Centrivap Jouan, ThermoFisher, USA) and
173 reconstructed in 40 µl of 25% aqueous acetonitrile (v/v). Five µl were injected onto Acquity
174 UPLC® CSHTM 1.7 µm, 2.1x150 mm chromatographic column and eluted using a gradient
175 elution of acidified water and acetonitrile. Data were acquired in a multiple reaction
176 monitoring mode. The detailed chromatographic and mass spectrometry conditions are
177 provided by Šimura et al. (2018). Data were processed with MassLynx V4.2 software (Waters,
178 Manchester, UK), and the concentrations of determined plant hormones were calculated
179 using the isotope dilution method. Endogenous IPyA was determined following the protocol
180 described by Pěnčík et al. (2018). Approximately 10 mg (fresh weight) samples were extracted
181 in 1 ml of cold 50 mmol/l phosphate buffer (pH 7.0) containing 0.1% sodium
182 diethyldithiocarbamate and isotope-labelled internal standard of IPyA. A 200 µl aliquot was
183 derivatised with cysteamine, acidified to pH 2.7 with HCl, and purified using in-tip µSPE. Eluted
184 samples were evaporated under reduced pressure, reconstituted in 10% aqueous methanol,
185 and analysed using an HPLC system 1260 Infinity II (Agilent Technologies, USA) equipped with
186 a Kinetex C18 column (50 mmx2.1 mm, 1.7 µm; Phenomenex) and coupled to 6495 Triple
187 Quad detector (Agilent Technologies, USA).
188
189 **ABA treatment**

190 ABA treatment was performed by culturing 15 siliques of 14 DAP and 18 DAP from HT and CT
191 conditions, respectively, collected from three plants in three biological replicates. The siliques
192 were cut at the pedicel region, collected, surface-sterilised with 70% ethanol, air dried, and
193 cultured in 50 ml tubes with 20 ml of ½ MS with 0.8% plant agar, 0.05% plant preservative for
194 tissue culture media (Plant Tissue Culture Technologies) and supplemented with 10 µM ABA
195 (Duchefa Biochemie) or the same volume of DMSO as negative control. A representative
196 picture of the cultured siliques is shown in Fig. S1. The silique culture was incubated in the
197 greenhouse with the other plants to simulate the same temperature conditions. The total,
198 viable, dead and SCR seed numbers were manually estimated on dried siliques under a Zeiss
199 stemi 305 stereomicroscope.
200
201 **RNA extraction and sequencing**
202 RNA was extracted from 50 mg of ground tissue of 14 DAP, 18 DAP, 20 DAP normal, and 20
203 DAP SCR seeds from CT and HT, collected from three plants in four biological replicates using
204 a NucleoSpin RNA Plant and Fungi kit (Macherey-Nagel) following the manufacturer's
205 protocol. The samples were treated with RNase-free rDNase (Macherey-Nagel) and repurified
206 using the RNeasy MinElute Cleanup Kit (Qiagen). The samples were sequenced by Novogene
207 Genomic Sequencing Labs. After sample quality control and library preparation, paired-end
208 short-read RNA sequencing was performed on poly-A RNA using an Illumina Novaseq
209 Sequencing platform. Quality check of raw paired-end fastq reads was carried out by FastQC
210 (Andrews, 2010), and their origin was categorised using BioBloomTools v2.3.4 (Chu *et al.*,
211 2014). The Illumina adapters and quality trimming of raw fastq reads were performed using
212 Trimmomatic v0.39 (Bolger *et al.*, 2014) with settings CROP:250 LEADING:3 TRAILING:3
213 SLIDINGWINDOW:4:5 MINLEN:35. Trimmed RNA-Seq reads were mapped to the *Brassica*
214 *napus* genome (genome build: Bra_napus_v2.0) with gene annotation (NCBI *Brassica napus*
215 Annotation Release 101) using STAR v2.7.3a (Dobin *et al.*, 2013) as splice-aware short read
216 aligner and default parameters except outFilterMismatchNoverLmax 0.1 and twopassMode
217 Basic. Quality control after alignment concerning the number and percentage of uniquely-
218 and multi-mapped reads, rRNA contamination, mapped regions, read coverage distribution,
219 strand specificity, gene biotypes, and PCR duplication was performed using RSeQC v4.0.0
220 (Wang *et al.*, 2012), Picard toolkit v2.25.6 (Picard toolkit, 2018), Qualimap v.2.2.2
221 (Okonechnikov *et al.*, 2016). All compatible results and statistics were processed by MultiQC

222 v1.10.1 (Ewels *et al.*, 2016). The sequence data have been deposited in the NCBI under the
223 Bio-Project PRJNA1188476 (https://www.ncbi.nlm.nih.gov/bioproject/PRJNA1188476).
224 The differential gene expression analysis was calculated based on the gene counts produced
225 using featureCounts from Subread package v2.0 (Liao *et al.*, 2014) and further analysed by
226 Bioconductor package DESeq2 v1.34.0 (Love *et al.*, 2014). Because of its conservative features
227 and to prevent false positive results, data produced by DESeq2 with independent filtering
228 were chosen for the differential gene expression analysis. Genes were considered to be
229 differentially expressed based on a cut-off for adjusted p-value ≤ 0.05 and log2FC ≥1 or ≤-1.
230 Clustered heatmaps were generated from selected top differentially regulated genes using R
231 package pheatmap v1.0.12 (Kolde, 2015), volcano plots were produced using ggplot2 v3.3.5
232 package (Wickham, 2011), and MA plots were generated using ggpubr v0.4.0 package
233 (Kassambara, 2018). GO enrichment is done taking all the Entrez gene IDs and cross-mapping
234 them against UniProt IDs, then taking all the transcript sequences and mapping them (using
235 BLAST) against the NCBI Nucleotide database subset for all species under taxons 3701
236 (A*rabidopsis* genus) and 981071 (*Brassicaceae* tribe) obtaining RefSeq gene IDs which were
237 cross-mapped against UniProt IDs and then used in GO enrichment. The co-expression cluster
238 analysis is described in Method S1.
239
240 **Seed embedding and sectioning**
241 Seeds were fixed in FAA (45% ethanol, 5% acetic acid and 1.85% formaldehyde) for 24 h under
242 vacuum, followed by another incubation at 4°C for 24 h in fresh FAA. The seeds were washed
243 once with water. Tissue softening was done with Franklin Maceration solution (1:1 v/v of 30%
244 H_2O_2 and glacial acetic acid) for 4 h at 60°C. Dehydration was done using 10, 20, 30, 40, 50,
245 60% ethanol series in 10% glycerine for 1 h at 30°C, followed by 4 days in 70% ethanol at 4°C
246 and dehydration with 80, 90 and 95% ethanol for 1 h at room temperature. Infiltration and
247 embedding with Technovit 7100 (Kulzer Technik Gmbh) were performed according to the
248 manufacturer's protocol with the following modifications. The initial infiltration was
249 performed in a 50% infiltration solution in ethanol overnight at room temperature, followed
250 by incubation for one week at 4°C in 100% infiltration solution with 1% w/v Technovit 7100
251 Hardener I. Embedding was performed with 6.6% w/v Technovit 7100 Hardener II in
252 infiltration solution and incubated for 8 days at -18°C to delay initial polymerisation. The
253 samples were then incubated at room temperature to complete the polymerisation process.

254 The 3-µm sections were prepared with a Leica RM2235 microtome using an attached
255 stainless-steel knife.
256
257 **Toluidine blue staining**
258 The sections were stained with 0.05% Toluidine blue (Acros Organics) for 1 minute, followed
259 by four washes of 3 minutes each. Mounting was done on dried slides with Entellan (Sigma-
260 Aldrich). Imaging of the sections was performed using a Zeiss AxioImager microscope. The
261 thickness of the seed coat layers was measured in twenty regions per section, for three
262 sections per seed and ten seeds per sample, using Image J. Graphs were plotted with
263 significance calculated using a two-way ANOVA test with Tukey multiple comparisons.
264
265 **Staining of lignin and pectin**
266 Seven seeds at 14 and 18 DAP from CT and HT and 22 DAP from CT were used. Pectin was
267 detected using a 0.05% w/v Ruthenium Red stain (Sigma-Aldrich) in an aqueous solution.
268 Sections were rehydrated before staining for 7 minutes, followed by two wash steps with
269 water, and mounted in Entellan (Sigma-Aldrich). Lignin was detected with 0.5% Safranin-O
270 (Acros organics) in an aqueous solution followed by three washes in water. Slides were
271 mounted in Entellan (Sigma-Aldrich). Imaging was done using a Zeiss AxioImager microscope.
272
273 **Immunolabelling**
274 Seeds at 10, 14, and 18 DAP from CT and HT, in two biological replicates, were fixed in 4% w/v
275 paraformaldehyde in ice-cold PEM buffer (50 mM PIPES, 5 mM EGTA, and 5 mM $MgSO_4$, pH
276 6.9). Samples were incubated on ice under vacuum for twice 1 h with fresh fixative solution,
277 followed by overnight incubation at 4°C. The samples were washed twice with ice-cold PEM
278 buffer, dehydrated through an ethanol series (50%, 70%, 80%, 90% and 100% three times)
279 under vacuum and infiltered with increasing concentrations (30%, 50% and 100%) of LR white
280 resin (Agar Scientific) in absolute ethanol over 8 days before being polymerised at 60°C for 24
281 h. Six seeds by timepoint per growth condition per biological replicate were sectioned (1 µm
282 thickness) using a glass knife mounted on a Leica RM2265 or EM UC7 microtome.
283 Immunolocalizations were performed with JIM5, LM19, LM20, and LM25 antibodies
284 (Agrisera). For immunolocalisation with LM25, an incubation with 0.1% pectolyase in 1X PBS
285 was done for 25 min at room temperature and washed once in 1X PBS before the blocking

286 step. For immunolocalisation with JIM5, LM19, and LM25, the sections were blocked with 3%
287 w/v BSA in 1X PBS and incubated for 1 h at room temperature. For the immunolocalisation
288 with LM20, an incubation in CAPS buffer (50 mM CAPS and 2 mM $CaCl_2$) for 1 h followed by
289 three washes with 1x PBS was performed before blocking with 3% skimmed milk in 1X PBS.
290 Sections were incubated with 1:10 v/v dilution of antibody prepared with 1% BSA in 1X PBS
291 for JIM5, LM19 and LM25 and 1% skimmed milk in 1X PBS for LM20 overnight at 4°C in a
292 humid chamber. The sections were brought to room temperature for 1 h, washed three times
293 with the above-mentioned buffers and incubated for 1 h in a humid chamber in the dark with
294 the secondary antibodies. A dilution of 1:100 v/v of secondary antibodies [anti-rat IgG Alexa
295 488 (Thermo Fisher) or anti-rat IgG Dylight 488 (Agrisera) for JIM5 and anti-rat IgM Dylight
296 488 (Thermo Fisher) for LM19, LM20 and LM25] in 1% BSA or 1% skimmed milk in 1X PBS was
297 used. Sections were washed in the respective buffers and 1X PBS, counterstained with 0.025
298 mg/ml Calcofluor white (Sigma-Aldrich), and mounted with VECTASHIELD antifade mounting
299 medium (Eurobio). The images were obtained with the ZEISS Axioimager 2 with a 40X dry
300 objective.
301 The intensity of the immunofluorescence in the cell walls of the epidermal and palisade layers
302 of the seed coat was quantified using ImageJ software. Images were adjusted using min/max
303 settings for optimal representation of fluorescent signals. For the three epidermal layers, a
304 segmented line with a width of 25 points was used to manually mark the cell walls of adjacent
305 cells of the same layer. The sum of fluorescence intensity in the three epidermal layers was
306 represented as one measurement. A region of interest was marked using the polygon
307 selection tool for the palisade layer. The mean fluorescence value obtained over the marked
308 regions for the different layers was subtracted from the background signal over the same area
309 to obtain the final fluorescence intensity.
310
311 **Cell wall profiling from the seed coat**
312 The enzymatic fingerprinting of the cell wall of seed coat from 10, 14 and 18 DAP seeds grown
313 under CT and HT conditions was performed in three biological replicates. The seed coats were
314 dissected from the seeds and were submerged in 96% (v/v) ethanol. The ethanol fraction was
315 discarded, and the seed coats were dried in a speed vacuum concentrator at 30°C overnight.
316 Dried seed coats were digested with 5 U/mg DW sample of *Pectobacterium carotovorum*
317 endo-polygalacturonase or *Paenibacillus* sp. xyloglucanase (Megazyme, Bray, Ireland) in 50

318 mM ammonium acetate buffer (pH 5) at 37°C for 18 h. Samples were centrifuged at 13,000
319 rpm for 10 min, and 100 µl of the supernatants were transferred into vials. For MS analysis,
320 10 µl of each fraction was injected. The oligosaccharides released from digestion were
321 separated according to Voxeur et al. (2019). Xyloglucan and pectin fragments were analysed
322 using an HPLC system (UltiMate 3000 RS HPLC system, Thermo Scientific, Waltham, MA, USA)
323 coupled to an Impact II Ultra-High Resolution Qq-Time-Of-Flight (UHR-QqTOF) spectrometer
324 (Bruker Daltonics, Bremen, Germany) equipped with an electrospray ionisation (ESI) source
325 in negative mode with the end plate offset set voltage to 500 V, capillary voltage to 4000 V,
326 nebuliser to 40 psi, dry gas to 8 l/min and dry temperature of 180°C. The Compass 1.8
327 software (Bruker Daltonics) was used to acquire the data. Chromatographic separation was
328 performed on an ACQUITY UPLC Protein BEH SEC Column (125A, 1.7 µm, 4.6 mm X 300 mm,
329 Waters Corporation, Milford, MA, USA) coupled with guard Column BEH SEC Column (125A,
330 1.7 µm, 4.6 mm X 30 mm). Elution was performed in 50 mM ammonium formate and 0.1%
331 formic acid at a flow rate of 0.4 ml/min and with a column oven temperature of 40°C.
332
333 **Space-restricted growth of siliques**
334 A 3-mm cross-section silicone tube was inserted over 10 DAP and 12 DAP siliques growing on
335 plants under HT and CT conditions, respectively, in three biological replicates with 20 siliques
336 per replicate. A 10 DAP silique at HT has a similar silique thickness to a 12 DAP silique at CT.
337 Siliques from the age and growth conditions without a silicone tube were used as a negative
338 control. The number of total, viable, dead and SCR seeds per dried silique were counted.
339
340 **Statistical analysis**
341 GraphPad Prism v.8.4.3 was used to plot the graphs and calculate the statistical significance
342 using either ANOVA or multiple comparison tests. R programming was used to analyse the
343 data and obtain the statistical significance for the RNA sequencing experiment.
344
345 **RESULTS**
346 ***Brassica napus* seed coat integrity is affected by long-term heat stress**
347 We have previously reported that in *Brassica napus* cv. Topas the early seed development is
348 affected under long-term heat treatment (HT) (Mácová *et al.*, 2022). This study focuses on
349 the seed coat rupture (SCR) observed in seeds of Topas developed under HT, starting at 20

DAP, while this phenomenon has never been observed in seeds grown under control treatment (CT) (Fig. 1a-e). The SCR phenotype occurred with variable outcomes, from a minor seed coat break with the embryo remaining intact within the seed to a complete testa rupture resulting in the embryo root or shoot protruding through the break site. Such embryos often had distinguishable phenotypes (Fig. 1c,d). The quantification of the phenotypes on dry seeds revealed a significantly reduced number of total viable seeds produced per silique, accompanied by a significant increase in the proportion of dead seeds and seeds with an SCR phenotype per silique in HT-grown siliques. At HT, approximately 50% of the seeds in a silique underwent SCR (Fig. 1e). Embryo staging of the seeds from 14 to 20 DAP indicated that embryo development is accelerated in seeds developed under HT compared to seeds grown under CT (Fig. 1f), which is consistent with our previous observations in seeds at early developmental stages (Mácová *et al.*, 2022). We estimated that the embryos in the seeds at HT were four days ahead of the embryos in seeds at CT in their developmental stage, e.g., a 14 DAP embryo at HT would be developmentally similar to an 18 DAP embryo at CT (Fig. 1f). Based on these observations, we designated 14 and 18 DAP HT seeds as early maturing seeds and HT seeds after 20 DAP as late maturing seeds.

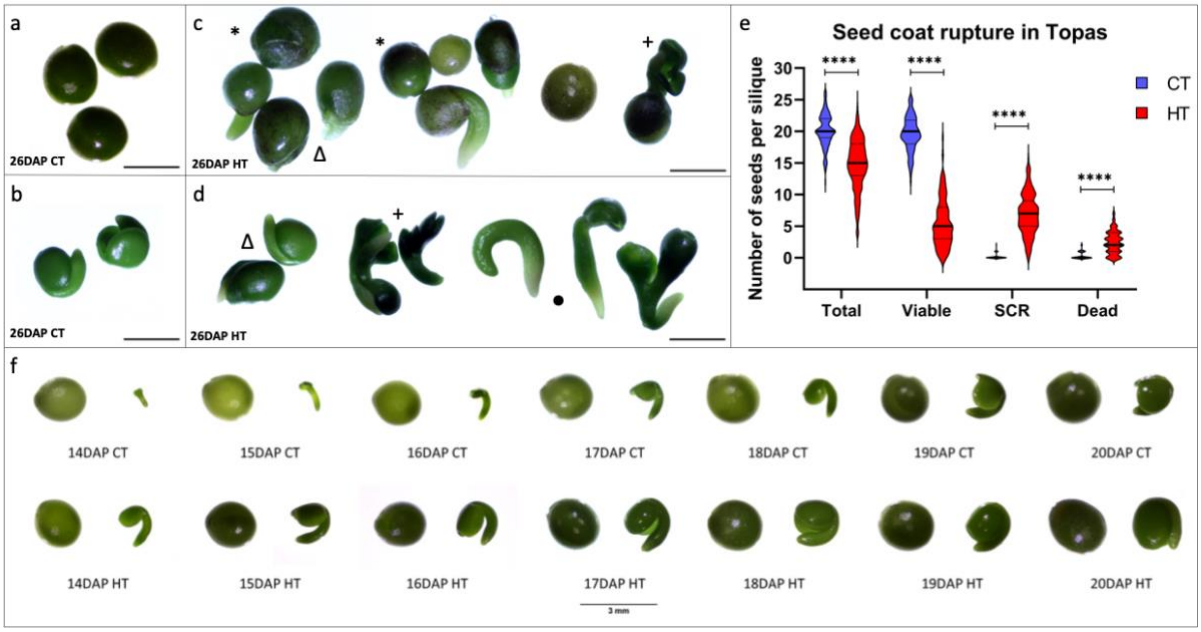

Fig. 1. SCR phenotype observed in Topas seeds developed under HT. (a, b) 26 DAP seeds (a) and their isolated embryos (b) grown under CT. (c, d) 26 DAP seeds (c) and their isolated embryos (d) grown under HT. SCR was observed (*, Δ, +, ●). * Indicates seeds with testa rupture with intact embryo, Δ indicates testa rupture with radicle protrusion, + indicates testa

372 rupture with cotyledon protrusion, and ● indicates embryos with abnormal development. (e)
373 Quantification of the number of dry seeds per silique from CT (blue) and HT (red) showing the
374 number of total, viable, SCR and dead seeds. Asterisks indicate statistically significant
375 differences in HT in a multiple t-test using the Holm-Sidak method (**** corresponds to *p*-
376 values of $p < 0.0001$. (f) Embryo stage of seeds developed on CT (top) and HT (bottom) from
377 14 to 20 DAP. The isolated embryo shown on the right is from the seed on the left. Scale bars:
378 2 mm (a-d) and 3mm (f).
379
380 **Unbalanced hormonal profiles of the seeds at HT may affect seed maturation**
381 The observed SCR phenotype led us to hypothesise that HT may deregulate seed dormancy
382 and maturation programs by affecting the homeostasis of the plant hormones abscisic acid,
383 gibberellins, and auxin. GA and its metabolites were below the detection limit, preventing any
384 conclusions about the influence of HT on their levels. In the seeds at 20, 26, and 36 DAP
385 developed under HT, ABA and IAA levels are significantly and age-dependently reduced (Fig.
386 2a; Fig. S2). The levels of the auxin precursor anthranilate (ANT) were significantly lower in 14
387 DAP HT embryos. In contrast, the levels of tryptophan (TRP) and indole-pyruvic acid (IPyA) in
388 14 DAP HT embryos and indole-3-acetonitrile (IAN) in 18 DAP HT embryos were significantly
389 higher compared to CT (Fig. S2). However, the levels of IAA in the CT and HT embryos at 14 or
390 18 DAP were not significantly different because the degradation products such as 2-
391 oxoindole-3-acetic acid (oxIAA) and IAA-aspartate (IAA-Asp) were significantly higher in the
392 embryos developed under HT. The levels of auxin metabolites in the seed coat were similar
393 to those observed in the embryos, except for a significant increase in IAA levels at HT. The IAA
394 levels were significantly reduced in mature seeds (20, 26 and 36 DAP). However, IAA levels in
395 intact and SCR seeds were not different (Fig. S2).
396 A significant increase in the levels of active ABA and its catabolic products (7-hydroxy-ABA,
397 phaseic acid (PA) and dihydrophaseic acid (DPA)) was observed in the embryos of 14 and 18
398 DAP seeds, whereas no significant changes were identified in the isolated seed coat (Fig. 2b).
399 When embryo stage was taken into account and ABA levels in 14 DAP embryos from HT were
400 compared with those in 18 DAP embryos from CT, no significant differences were found. ABA
401 levels were significantly reduced in 26 and 36 DAP mature seeds developed under HT, with
402 no significant difference between intact and SCR seeds (Fig. 2a). These reduced ABA and IAA
403 levels in mature seeds led to the hypothesis of reduced seed dormancy in HT.

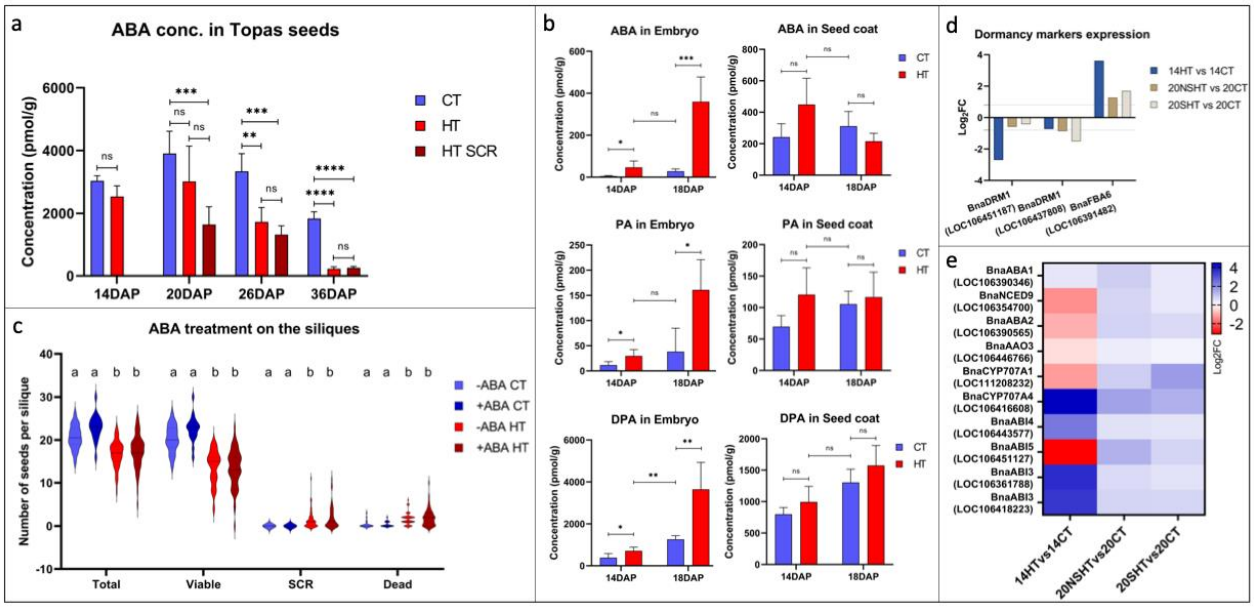

Fig. 2. ABA levels and expression of genes involved in ABA metabolism in *Brassica napus* Topas seeds. (a) Seeds were from 14 DAP to 36 DAP of CT (blue) and HT (red, dark red). From 20 DAP, HT seeds were separated into intact seeds (red) and SCR seeds (dark red). Quantification is presented as pmol per g fresh weight. (b) Measurements were performed for ABA, phaseic acid (PA), and dihydrophaseic acid (DPA) from embryos and seed coats from 14 DAP and 18 DAP seeds grown in CT (blue) and HT (red). Asterisks indicate statistically significant differences in HT and between 14 DAP HT and 18 DAP CT in a multiple t-test using the Holm-Sidak method (*, **, *** and **** correspond to *p*-values of $0.05 > p > 0.01$, $0.01 > p > 0.001$, $0.001 > p > 0.0001$ and $p < 0.0001$, respectively); n.s., not significant. (c) 15 siliques of 14 DAP and 18 DAP from HT and CT, respectively, were cultured in the presence or absence of 10 µM ABA (Fig. S1). Dry seeds were quantified for the number of total viable, SCR and dead seeds per silique. Samples with the same letter were not statistically significantly different. (d) Relative expression of selected genes representing DORMANCY ASSOCIATED gene 1 (DRM1) and FRUCTOSE 1,6-BIPHOSPHATE ALDOLASE 6 (FBA6) in 14 DAP (blue), 20 DAP intact (yellow) and 20 DAP SCR (grey) seeds. Data were extracted from the transcriptome dataset (Tables S1 and S2). (e) Heatmap showing the differential expression of selected genes involved in ABA metabolism in 14 DAP, 20 DAP intact, and 20 DAP SCR seeds. The full dataset is provided in Tables S1 and S2.

ABA treatment on the siliques did not restore the SCR phenotype

425 To test whether the reduced ABA in the seeds was one of the causes of the SCR phenotype
426 and reduced seed dormancy at HT, we cultured the Topas siliques in the presence of 10 µM
427 ABA in an *in vitro* silique culture experiment. The number of seeds undergoing SCR at HT in
428 the siliques cultured with ABA was not significantly different from that in untreated siliques
429 (Fig. 2c). Moreover, *in vitro* silique culture appeared to partially rescue SCR at HT compared
430 to seeds developed in siliques attached to the plants, most likely due to the increased
431 humidity of the culture setup (Fig. S1). Thus, the cultured siliques produced more viable seeds.
432 Comparable results were observed with different modes of exogenous application of ABA to
433 individual siliques and in an *in vitro* seed culture (data not shown).
434
435 **The embryo-to-seed size ratio is increased at HT**
436 We observed that seed development in Topas and Westar was accelerated under long-term
437 high-temperature growth, with embryos exhibiting a four-day advance in maturity under HT
438 compared to CT (Fig. 1, Fig. S3, Mácová et al., 2022). The SCR rate for Topas seeds was higher
439 than that for Westar seeds (Mácová *et al.*, 2022). We hypothesised that this accelerated
440 embryo growth may interfere with seed development, thereby inducing the SCR phenotype.
441 We compared seed area and embryo area in seeds from 14 to 20 DAP at CT and HT in both
442 cultivars. The seed area increased from 14 to 20 DAP, and this increase was reduced from 20
443 DAP as the seeds entered the maturation phase (Fig. 3a, c). In Topas, the seed size at 18 DAP
444 was significantly larger under HT than under CT (Fig. 3a). In Westar, seeds were slightly larger
445 under HT at 14 DAP and smaller at 20 DAP (Fig. 3c). It should be noted that the seeds of the
446 Westar cultivar were larger on average than those of the Topas cultivar. Embryos at HT were
447 more than twice the size of those at the same DAP at CT for each DAP in both cultivars (Fig.
448 3b, d). These observations suggest that the seeds did not undergo a compensatory increase
449 in size to accommodate the HT-induced enlargement of the embryos. The embryo-to-seed
450 area ratio provides valuable insight into the space occupied by the embryo within the seed at
451 a given DAP under the two growth conditions (Fig. 3e). We observed that the embryos
452 developed under HT filled significantly more space in the seed than those grown under CT.
453 Furthermore, the embryo-to-seed area ratio in Topas was significantly higher than that in
454 Westar at 20 DAP. These observations suggest that the accelerated embryo growth in HT
455 resulted in the formation of larger embryos but not larger seeds.
456

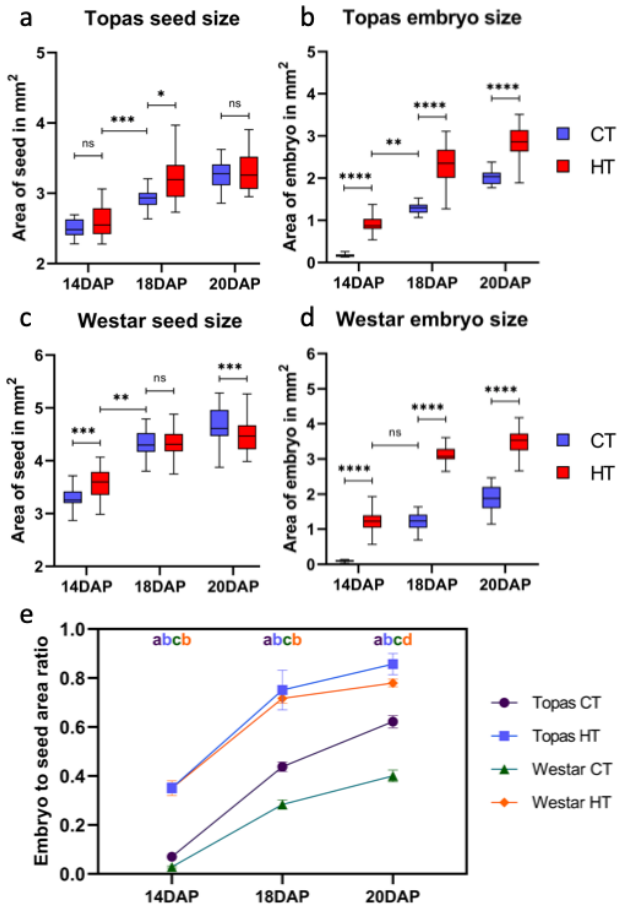

Fig 3. Embryo and seed size measurements of *Brassica napus* Westar and Topas seeds developed at CT and HT. (a, b) Seed (a) and embryo (b) area measurements in mm^2 of 14, 18 and 20 DAP Topas seeds developed at CT (blue) and HT (red). (c, d) Seed (c) and embryo (d) area measurements in mm^2 of 14, 18 and 20 DAP Westar seeds developed at CT (blue) and HT (red). Asterisks indicate statistically significant differences in HT and between 14 DAP HT and 18 DAP CT in a two-way ANOVA test with Sidak's multiple comparisons (*, **, *** and **** correspond to *p*-values of $0.05 > p > 0.005$, $0.005 > p > 0.0005$, $0.0005 > p > 0.0005$ and $p < 0.00005$, respectively); n.s., not significant. (e) Embryo-to-seed size ratio in 14, 18 and 20 DAP Topas and Westar seeds developed at CT and HT. Samples with the same letter were not statistically significantly different. Representative pictures of the seeds and embryos are shown in Fig. S3.

The formation of larger embryos at HT impacts the thickness of the seed coat cells

We wondered whether the presence of larger embryos in these seeds might affect the seed coat cells, leading to SCR. The seed coat of *B. napus* is composed of three layers of cells (Fig.

4a): an outer epidermal layer of three cell files, a middle palisade layer made of a single layer of cells with substantial secondary cell walls, and an inner endothelial layer surrounding the endosperm (Jiang & Deyholos, 2010). The thickness of these three layers of the seed coat was measured in seeds of 10, 14, 18, 20, and 22 DAP developed under CT and HT (Fig. 4f-h). Seed coat thickness was not affected by HT in 10 DAP seeds (Fig. 4f-h). However, all three seed coat layers were significantly thinner in older seeds developed under HT (Fig. 4b-h). The palisade and the first endothelial layers were the most affected by this reduction, with a 46% reduction in endothelial cell layer thickness induced by HT as the seed aged from 14 DAP to 20 DAP, whereas the thickness reduction was only 12% at CT (Fig. 4i). These results indicate that the HT-induced embryo growth from 14 DAP increased tension on the cells of the developing seed coat, reducing its thickness due to cell stretching.

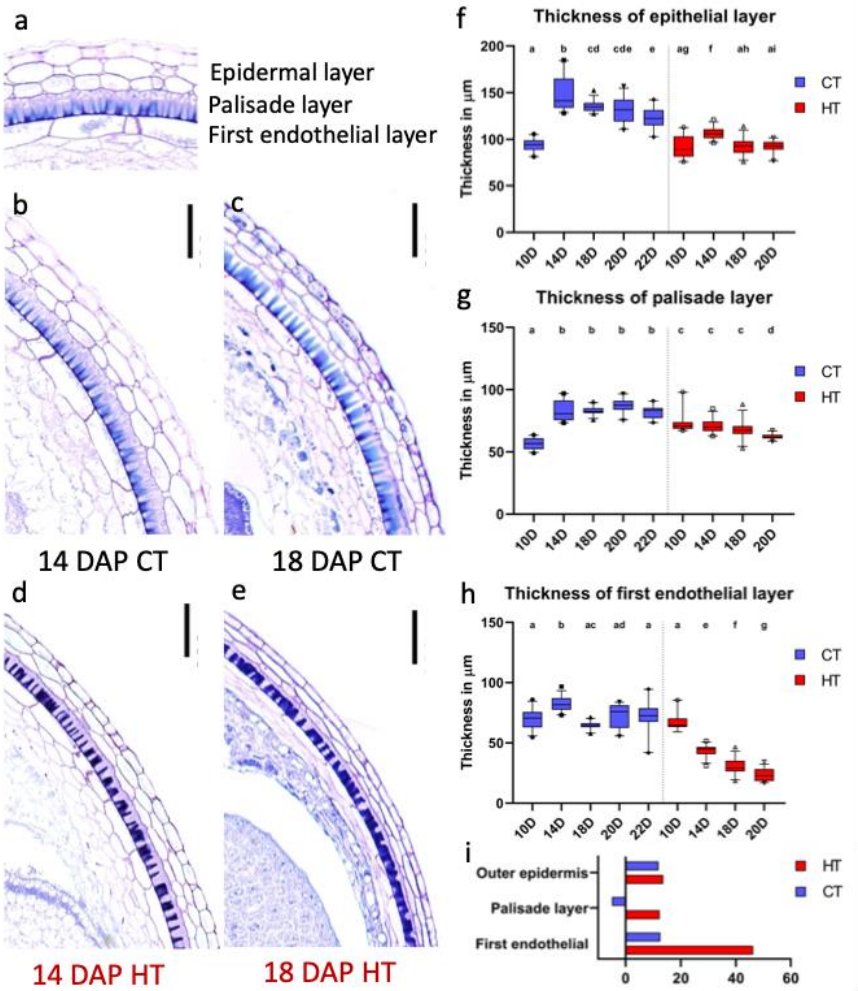

Fig. 4 The thickness of the seed coat cells is reduced in HT. (a-e) Histological sections of Topas seeds focused on the seed coat, stained with toluidine blue. (a) The seed coat is composed of an epidermal layer, a palisade layer and an endodermal layer. (b-e) Seed coat of 14 DAP seeds

488 from CT (b) and HT (d) and 18 DAP seeds from CT (c) and HT (e). Scale bars represent 200 µm.
489 (f-h) Box-whisker plots show the size mean, median, outliers, and SD in µm of the thickness
490 of the epidermal layer (f), palisade layer (g) and first endothelial cell layer (h) in 10, 14, 18,
491 and 20 DAP seeds from CT (blue) and HT (red). Samples with the same letter were not
492 statistically significantly different. (i) Percentage of reduction in thickness as the seed aged
493 from 14 to 20 DAP.
494
495 **Transcriptional regulation of the dormancy regulators provides a conflicting picture of the**
496 **HT effects on seed dormancy**
497 To gain an insight into the molecular mechanisms of SCR at HT in Topas, we performed
498 transcriptional profiling of seeds developed under HT and CT conditions at 14, 18 and 20 DAP,
499 including seeds without (20NSHT samples) and seeds with (20SHT samples) SCR phenotypes
500 at 20 DAP. Principal component analysis (PCA) using gene expression data from all the
501 samples was used to test for differences between samples and biological replicates. The PCA
502 revealed that the 14 DAP HT samples clustered with the 18 and 20 DAP CT samples,
503 correlating with the advanced embryo stage of the 14 DAP HT seeds (Fig. 5a). High-quality
504 clean reads were used for the differential expression gene (DEG) and gene ontology (GO)
505 enrichment analysis. Many misregulated (up- and down-regulated) DEGs, shown as Venn
506 diagrams (Fig. S4), were identified in our comparisons of samples from the same DAP: 14HT
507 vs. 14CT, 18HT vs. 18CT, and 20NSHT vs. 20SHT and 20CT, and of samples from the same
508 embryo stage (14HT vs. 18CT). The significant GO terms associated with the transcriptional
509 response of the seeds to HT conditions are related to cell cycle, development, hormonal
510 regulation, heat stress and changes in metabolic pathways (Fig. S5, Table S3).
511 To better understand the relationship between the HT-induced SCR phenotype, hormonal
512 deregulation, and seed dormancy, we first focused the analysis on the differential expression
513 of the dormancy gene markers DORMANCY ASSOCIATED gene 1 (DRM1) (Rae *et al.*, 2013) and
514 FRUCTOSE 1,6-BIPHOSPHATE ALDOLASE 6 (FBA6) (Lu *et al.*, 2012), genes involved in ABA
515 metabolism and signalling, and previously identified transcription factors involved in
516 dormancy regulation. We did not observe any significant difference between the 20SHT and
517 20NSHT (Fig. 2d,e; Fig. 5b; Table S2), possibly because the molecular information leading to
518 the SCR might already be encoded in younger seeds. The BnaDRM1 LOC106451187 and
519 LOC106437808 genes are highly expressed in dormant tissues (Rae *et al.*, 2013) and were

520 downregulated in 14HT and 20HT seeds (Fig. 2d). The BnaFBA6 LOC106391482 gene, which is
521 involved in the sugar metabolism pathway (Lu *et al.*, 2012), was upregulated in 14HT and
522 20HT seeds. The misregulation of these two dormancy markers indicates that seeds under HT
523 may have a reduced dormancy state. Expression of the following enzymes involved in ABA
524 biosynthesis (Wu *et al.*, 2023), zeaxanthin epoxidase BnaABA1 (LOC106390346), 9-cis-
525 epoxycarotenoid dioxygenase BnaNCED9 (LOC106354700), dehydrogenase reductase
526 BnaABA2 (LOC106390565), and abscisic aldehyde oxidase BnaAAO3 (LOC106446766), was
527 significantly lower at 14HT but no significant differences were observed as seeds matured
528 from 14 to 20 DAP (Fig. 2e). The expression of BnaCYP707A1 (LOC111208232) and
529 BnaCYP707A4 (LOC106416608), which are involved in the ABA degradation pathway to form
530 PA and DPA, was significantly increased at 20SHT (Fig. 2e), which correlated with the reduced
531 ABA concentration in 20 DAP seeds from HT (Fig. 2a). Although the expression profiles of
532 genes involved in ABA metabolism support the reduced ABA levels in the seeds under HT, the
533 expression of ABA signalling genes BnaABI3 (LOC106361788 and LOC1064188223) and
534 BnaABI4 (LOC106443577), which promote seed dormancy, was increased in 14HT seeds,
535 while BnaABI5 (LOC106451127) was decreased (Fig. 2e). In older seeds, their expression was
536 not affected by HT. We further examined the expression pattern of some transcription factors
537 reported to regulate seed dormancy and seed germination. The expression of the AUXIN
538 RESPONSE FACTORs ARF10 and ARF16, which directly promote the expression of ABI3 (Liu *et*
539 *al.*, 2013) was not significantly changed in any of the comparisons (Fig. 5b). The AP2
540 transcription factor CHOTTO 1 (CHO1)/PLETHORA 5 (PLT5)/AINTEGUMENTA-like 5 (AIL5) acts
541 downstream of ABI4 during seed germination (Yamagishi *et al.*, 2009; Yano *et al.*, 2009).
542 Similar to ABI4, its expression was upregulated at 14HT and insignificant at 20 DAP (Fig. 5b).
543 DELAY OF GERMINATION 1 (DOG1) (Carrillo-Barral *et al.*, 2020), REDUCED DORMANCY 5
544 (RDO5)/DOG18 (Xiang *et al.*, 2014), RGA-like 2 (RGL2), and PHYTOCHROME INTERACTING
545 FACTOR 3-like 5 (PIL5) (Oh *et al.*, 2007), which are reported to promote dormancy, and
546 SPATULA (SPT) (Vaistij *et al.*, 2013), which plays an antagonistic role in dormancy regulation,
547 were up-regulated in 14HT, 18HT and 20HT seeds (Fig. 5b; Fig. S6; Table S4). HONSU, a seed-
548 specific protein phosphatase 2C that negatively regulates seed dormancy (Kim *et al.*, 2013),
549 was up-regulated in 14HT seeds, but down-regulated in later stages (Fig. 5b). The regulators
550 and markers of seed germination were up-regulated in HT seeds, supported by the overall
551 reduction in ABA levels in the whole seeds entering the maturation stage. However, the

552 regulators of seed dormancy were also up-regulated at all stages. These data suggest that the
553 transcriptional behaviour of seed dormancy and germination regulators in HT-developing
554 seeds is contradictory, making it difficult to draw conclusions.

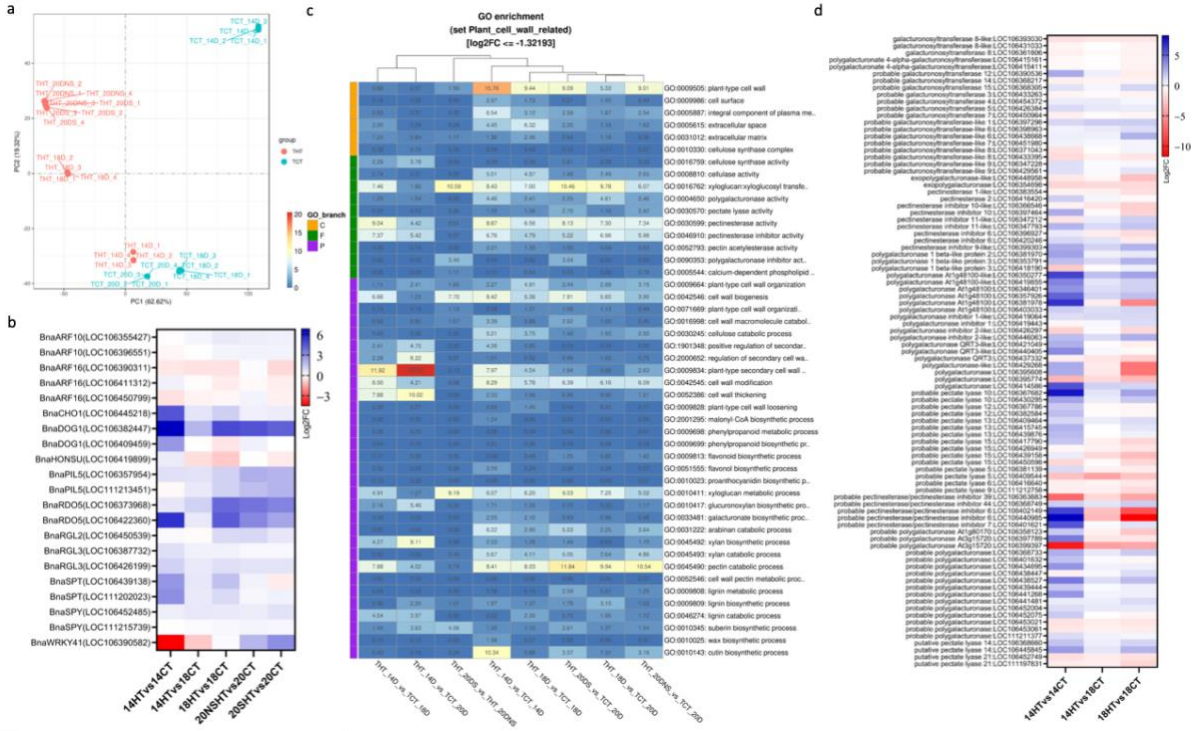

555

556 **Fig. 5** Transcriptional changes in Topas seeds associated with growth at HT indicate changes
557 in cell wall composition. (a) Principal component analysis using gene expression data from the
558 samples tested for differences between samples and biological replicates. (b) Heatmap
559 showing differential transcription of selected genes involved in seed dormancy in 14 DAP, 18
560 DAP, 20 DAP intact and 20 DAP SCR seeds. Expression in 14 DAP HT seeds is compared with
561 expression in 18 DAP CT seeds. (c) GO terms related to cell wall associated with the
562 transcriptional response of Topas seeds to HT are shown. (d) Heatmap showing the
563 differential transcription of selected genes involved in pectin metabolism in 14 and 18 DAP
564 seeds grown at CT and HT. The expression in 14 DAP HT seeds is compared with the expression
565 in 18 DAP CT seeds. The full dataset is presented in Tables S1, S2 and S3.

566

567 **The composition and properties of the seed coat cell wall are altered in HT-grown seeds**

568 Gene ontology enrichment analysis revealed significant misregulation in many pathways
569 related to plant cell walls (Fig. 5c). Interestingly, these included secondary cell wall biogenesis,
570 cell wall thickening and modification, cellulose, pectin, and xyloglucan metabolism and
571 modification pathways. Looking at the DEGs associated with pectin metabolic pathways, we

572 identified in 14HT and 18HT seeds the misregulation of enzymes such as
573 galacturonosyltransferases (GAUT) involved in pectin biosynthesis (Mohnen, 2008),
574 pectinmethylesterases and pectinmethylesterase inhibitors, involved in the chemical
575 modifications of pectin (Wormit & Usadel, 2018; Wu *et al.*, 2018; Xu *et al.*, 2022), and
576 polygalacturonases and pectate lyases, involved in pectin degradation (Marin-Rodriguez,
577 2002; Park *et al.*, 2010; Safran *et al.*, 2023) (Fig. 5d). This suggests that heat stress may
578 regulate the chemical modification of pectin, a major constituent of the cell wall.
579 To confirm whether the transcriptional changes in the cell wall-modifying enzymes affect the
580 pectin and lignin levels in the seed coat of HT-grown seeds, we used Ruthenium Red, which
581 stains the polyanionic molecules in the deesterified monomers of pectin in red (Nagayama *et*
582 *al.*, 2019), and Safranin-O, which has a high affinity for the phenolic compounds in lignin and
583 stains the walls bright red (Bond *et al.*, 2008) (Fig. 6a,b). The cells of the palisade layer in the
584 seed coat of 14 and 18 DAP Topas seeds grown under HT were strongly stained red with
585 Ruthenium Red and Safranin-O compared to the 14, 18 and 22 DAP seeds grown under CT.
586 The staining intensity increased with seed age. These observations suggest that seeds
587 entering the maturation phase accumulate more secondary cell wall elements in the seed
588 coat in HT than in CT.
589 Seed coat cell wall composition determines its mechanical strength (Mendu *et al.*, 2011;
590 Sechet *et al.*, 2018). The presence of pectin and hemicellulose in the seed coat layers was
591 investigated by immunostaining the seed coat with selective antibodies (Fig. 6d-g). For pectin,
592 which is mainly made of homogalacturonan (HG), we used the antibody LM19 that binds
593 preferentially to demethylesterified HG, the antibody LM20 that binds preferentially to
594 methylesterified HG, and the antibody JIM5, which has a high affinity for partially
595 demethylesterified HG (Fig. 6d-f). For hemicellulose, composed mainly of xyloglucan, the
596 LM25 antibody was used and combined with a pectolyase treatment to digest the pectin that
597 masks the hemicellulose (Fig. 6g). Fluorescence was quantified in the epidermal and palisade
598 layers of the seed coat. The seed coats of HT-developed 14 and 18 DAP seeds had significantly
599 higher levels of fluorescence of the LM19 and JIM5 antibody signals in the palisade layer,
600 indicating an increase in demethylesterified HG. In contrast, no significant differences in the
601 fluorescence intensity of the LM20 antibody signal were found in the cells of the palisade
602 layer in the testa of CT and HT seeds. In the epidermal layer of seeds developed under HT, the
603 signal for the JIM5 and LM19 antibodies was significantly higher in 14 DAP seeds, whereas the

604 signal for the LM20 antibody was significantly reduced at 18 DAP, indicating a reduction in
605 the amount of methylesterified HG. The results indicate an early enrichment of pectin and an
606 early shift towards demethylesterified pectin in the cell walls of the palisade and epidermal
607 cells in 14 DAP seeds grown under HT, with a significant reduction in the amount of
608 methylesterified HG molecules. LM25 fluorescence was significantly higher only in the
609 palisade cells of 18 DAP HT-grown seeds compared to CT seeds, suggesting a slight effect of
610 temperature on the amount of xyloglucan in the seed coat of these seeds (Fig. 6g).
611 To confirm our microscopic observations, we performed enzymatic fingerprinting of the cell
612 wall of the isolated seed coats from 10, 14 and 18 DAP seeds of Topas grown at CT and HT.
613 Digestion of HG by an endo-polygalacturonase between unmethylesterified ester stretches of
614 the galacturonic acid (GalA) releases several oligogalacturonans (OGs). OGs have been termed
615 GalAxMeyAcz based on the degree of polymerisation of GalA and the number of methyl and
616 acetyl groups. In our analysis of the Topas seed coat, we identified GalA3, GalA3ox, GalA3Xyl,
617 GalA3Me, GalA3MeAc, GalA4Ac, GalA4Me, GalA4Meox, GalA4Me-H_2O, and DPx>4Mey
618 (methylesterified OGs with degree of polymerisation greater than 4). The total peak area
619 obtained from the MS analysis was plotted by grouping OGs with and without methyl groups
620 (Fig. 6h). A significant increase of unmethylesterified OGs was released from the cell walls of
621 14 DAP seed coat at HT compared to CT, which correlates with the signal intensity of the LM19
622 antibody binding to the unmethylesterified HGs in the cell walls in the seed coat layers (Fig.
623 6i,j). Similarly, a significant increase in the methylesterified OGs in the seed coats of 14 DAP
624 with varying numbers of methyl groups correlates with the signal intensity of JIM5 antibody
625 binding to partially methylesterified HGs in the cell walls of the epidermal and palisade layers
626 (Fig. 6i,j). It is worth noting the release of oxidized OGs, which might reflect the presence of
627 long oxidized OGs trapped with the pectin and not solubilized through alcohol extraction.
628 Regarding xyloglucan, LXXGAc levels did not change significantly and correlated with LM25
629 signal in the seed coat (Fig. 6k,l). However, a significant increase in the level of fucosylated
630 subunits is observed in the 14 DAP seed coats of HT compared to CT (Fig. 6k).
631 Using a variety of approaches, we found that growth on HT modified the cell wall properties
632 in the seed coat of seeds from 14 DAP onwards. The cell walls of the epidermal and palisade
633 cells accumulate more pectin and shift prematurely towards the production of
634 demethylesterified pectin, possibly making the cell wall stiffer.
635

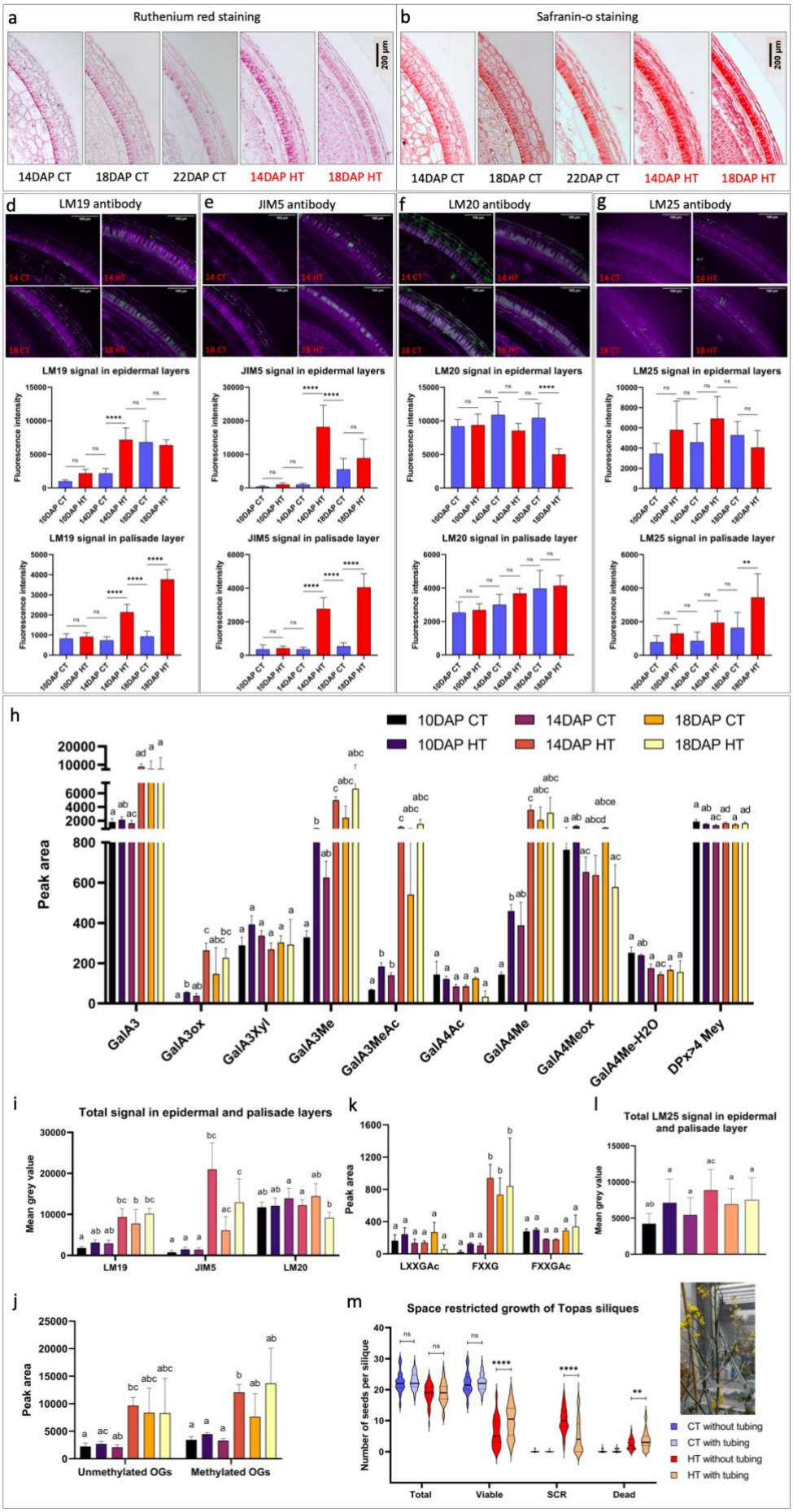
a
Ruthenium red staining
200 µm
14DAP CT
18DAP CT
22DAP CT
14DAP HT
18DAP HT
b
Safranin-o staining
200 µm
14DAP CT
18DAP CT
22DAP CT
14DAP HT
18DAP HT
d
LM19 antibody
e
JIM5 antibody
f
LM20 antibody
g
LM25 antibody
LM19 signal in epidermal layers
JIM5 signal in epidermal layers
LM20 signal in epidermal layers
LM25 signal in epidermal layers
LM19 signal in palisade layer
JIM5 signal in palisade layer
LM20 signal in palisade layer
LM25 signal in palisade layer
Fluorescence intensity
10DAP CT
10DAP HT
14DAP CT
14DAP HT
18DAP CT
18DAP HT
h
10DAP CT
10DAP HT
14DAP CT
14DAP HT
18DAP CT
18DAP HT
Peak area
GalA3
GalA3ox
GalA3Xyl
GalA3Me
GalA3MeAc
GalA4Ac
GalA4Me
GalA4Meox
GalA4Me-H2O
DPx>4 Mey
i
Total signal in epidermal and palisade layers
Mean grey value
LM19
JIM5
LM20
k
Peak area
LXXGAc
FXXG
FXXGAc
l
Total LM25 signal in epidermal and palisade layer
Mean grey value
j
Peak area
Unmethylated OGs
Methylated OGs
m
Space restricted growth of Topas siliques
Number of seeds per silique
Total
Viable
SCR
Dead
CT without tubing
CT with tubing
HT without tubing
HT with tubing

636

637 **Fig. 6** The composition and properties of the seed coat cell wall are altered in HT-grown seeds.
638 (a, b) Histological sections of Topas seeds focused on the seed coat, stained with Ruthenium
639 Red for pectin (a) and Safranin-O for lignin (b). Sections of 14, 18, and 22 DAP CT seeds and
640 14 and 18 DAP HT seeds are shown. Scale bars represent 200 µm. (d-g) Immunolocalization
641 of pectin and xyloglucans using LM19, JIM5, LM20 and LM25 antibodies on the testa of 14
642 and 18 DAP HT and CT seeds. The signal is visible in green, the cell structure is marked in
643 magenta with calcofluor white. Scale bars represent 100 µm. Fluorescence intensity was
644 measured in epidermal and palisade cells in 10, 14 and 18 DAP HT and CT seeds. Asterisks
645 indicate statistically significant differences in HT and between seed ages in a one-way ANOVA
646 test with Tukey multiple comparisons (*, **, *** and **** correspond to *p*-values of $0.05 > p$
647 > 0.01, $0.01 > p > 0.001$, $0.001 > p > 0.0001$ and $p < 0.0001$, respectively); n.s., not significant.
648 (h) Pectin composition of the seed coat cell wall of 10, 14, and 18 DAP seeds from HT and CT.
649 The graph shows the measurements expressed as peak area from the MS analysis for GalA3,
650 GalA3ox, GalA3Xyl, GalA3Me, GalA3MeAc, GalA4Ac, GalA4Me, GalA4Meox, GalA4Me-H_2O
651 and DPx>4Mey (methylesterified OGs with degree of polymerisation greater than 4). (i) Graph
652 showing the total intensity signal for pectin from (d-f). (j) Graph showing the amount grouped
653 as methylesterified versus non-methylesterified OGs from (h). (k) Graph showing the
654 measurements presented as peak area from the MS analysis for xyloglucans. (l) Graph
655 showing the total intensity signal for xyloglucan from (g). Samples with the same letter were
656 not statistically significantly different. (m) A 3-mm silicon tube was applied to siliques from 10
657 DAP CT and 12 DAP HT. Dry seeds were quantified for the number of total viable, SCR and
658 dead seeds per silique. Asterisks indicate statistically significant differences in HT and
659 between seed ages in a two-way ANOVA test with Tukey multiple comparisons (*, **, *** and
660 **** correspond to *p*-values of $0.05 > p > 0.01$, $0.01 > p > 0.001$, and $p < 0.001$, respectively);
661 n.s., not significant.
662

663 **Application of mechanical constraints during silique development partially rescues SCR**
664 **phenotype**

665 Since the seed coat thickness of seeds developed under HT was significantly reduced, we
666 suspected that such a seed coat would lack the strength to accommodate the developing
667 embryo. The continuous embryo growth would exert additional mechanical pressure on the
668 seed coat, resulting in SCR. To verify this, we applied a silicone tube to developing siliques to

provide an external mechanical constraint on the seeds in an attempt to compensate for the early embryonic pressure on the seed coat (Fig. 6m). Such an experiment was previously performed to show that an applied mechanical force on the siliques triggers seed maturation by arresting embryonic growth (Rolletschek *et al.*, 2024). The presence of the silicone tube on the siliques of CT plants did not affect the seed viability or promote SCR. In HT, the external force exerted by the silicone tube on the silique (and thus on the seeds inside) resulted in a significant decrease in the number of seeds undergoing SCR and an increase in the number of viable seeds (Fig. 6m). The application of an external mechanical support reinforced the compromised mechanical strength of the seed coat caused by the faster embryo development.

DISCUSSION

Rising global temperatures adversely affect the production of major staple crops (Agnolucci *et al.*, 2020; Jägermeyr *et al.*, 2021), by hindering proper seed development, as in *Brassica napus* (Mácová *et al.*, 2022). The occurrence of temperature-induced preharvest seed sprouting was reported in our previous study in three spring cultivars of *B. napus* (Mácová *et al.*, 2022). In particular, prolonged cultivation of Topas at temperatures above the suboptimal temperature resulted in half of the seeds per silique undergoing SCR. In this study, we have elucidated the molecular mechanism behind the regulation of the SCR phenotype that occurs in Topas during seed maturation.

Genetic screens in *Arabidopsis* have identified the molecular components involved in seed maturation and dormancy (Finkelstein *et al.*, 2002; Holdsworth *et al.*, 2008). Reduced ABA levels or increased levels of active GAs result in reduced seed dormancy (Benech-Arnold & Rodríguez, 2018; Tai *et al.*, 2021). Although HT conditions during seed maturation (after 20 DAP) in Topas resulted in reduced ABA levels, suggesting reduced seed dormancy, there were no differences between SCR and non-SCR seeds. Furthermore, the failure of *in vitro* ABA treatment to rescue SCR led to the hypothesis of a minimal role for ABA in SCR. No direct conclusions could be drawn linking the state of dormancy to the SCR phenotype, as even the genes reported to positively regulate seed dormancy, such as *ABI3, ABI4, DOG1, RDO5, CHO1*, and *SPT*, have increased expression levels in seeds developed on HT, but still lead to SCR.

Growth at elevated temperatures accelerated embryo development in *B. napus* from early developmental stages (Mácová *et al.*, 2022). Indeed, most of the embryos from 6 DAP seeds

701 produced at optimal growth temperature were at the 8-cell stage, whereas at elevated
702 temperatures, they were at the mid to late globular stage. A similar difference was observed
703 in the maturation phase, with a difference of 4 days for equivalent developmental stages. As
704 a result, embryos were larger in seeds that did not enlarge, possibly exerting mechanical
705 pressure on the seed coat. Mechanical constraints applied to developing seeds of *B. napus* cv.
706 Reston promoted seed maturation by activating the storage metabolism and the expression
707 of genes involved in the embryo maturation process (Rolletschek *et al.*, 2024). The higher
708 levels of ABA in 14 and 18 DAP embryos developed under HT and the increased expression
709 pattern of *ABI3* and *DOG1* in HT seeds during early maturation suggest that seed development
710 under elevated growth temperature could promote an early maturation process (Baud *et al.*,
711 2016; Leprince *et al.*, 2016; Rolletschek *et al.*, 2024).
712 The proper exchange of signals between the seed coat, endosperm, and embryo interacts to
713 define the final size, shape, and dormancy state of the seed at the end of the maturation
714 phase (Li *et al.*, 2019). The *Arabidopsis iku2-2 zou-4* double mutant has reduced seed viability
715 due to developing seeds undergoing testa rupture (Creff *et al.*, 2015), similar to the SCR
716 phenotype observed in Topas. The mutation in *HAIKU2 (IKU2)* results in increased endosperm
717 pressure, favouring mechanosensitive precocious testa stiffening, possibly dependent on
718 demethylesterified pectin accumulation. This results in small *iku2* seeds (Creff *et al.*, 2023).
719 Seeds of *zhoupi-4 (zou-4)* have a persistent endosperm at the torpedo stage, even as the
720 embryo expands in size, producing large seeds during development (Creff *et al.*, 2015). Testa
721 rupture in *iku-2 zou-4* seeds would be a consequence of early testa stiffening together with
722 increased pressure from the developing embryo and a persistent endosperm. Both *IKU2* and
723 *ZOU* expression were down-regulated in Topas seeds developed at high temperatures (Fig. S6
724 and Table S2), suggesting that a similar process may occur in *B. napus*.
725 GO enrichment analysis of the seed transcriptome revealed a temperature-dependent
726 misregulation of cell wall-related pathways in seeds. Pathways related to cellulose, pectin and
727 xyloglucan metabolism, cell wall thickening, and pectin modification were overrepresented.
728 The primary cell wall is composed of cellulose, hemicellulose, and pectin (Cosgrove, 2024),
729 while the secondary cell wall can be stiffened with lignin. Cellulose and hemicellulose are
730 embedded in a gel matrix formed by pectin and influence the extensibility of the cell wall, an
731 essential feature for cell growth and morphogenesis (Peaucelle *et al.*, 2011). Many genes
732 involved in pectin biosynthesis, modification, and degradation were misregulated, which led

us to investigate the methylesterification pattern of pectin, which could influence wall rheology. Ruthenium Red staining for pectin and Safranin-O staining for lignin indicated that both pectin and lignin levels were increased in the palisade layer of HT seed coats. Immunostaining with pectin-specific antibodies and cell wall profiling of the seed coat of early maturing seeds indicated that the overall pectin composition was altered, particularly in the palisade layer. The significant enrichment of demethylesterified pectin in the palisade layer of early maturing seeds developed under HT suggests that the seed coat cell walls may be stiffer when grown at elevated temperatures.

The embryo stage and size difference observed in HT seeds may exert increased pressure on the walls of the developing seed coat for the same overall seed size, resulting in increased tension between adjacent cells within an integument layer. The reduction in the thickness of the epidermal, palisade and endothelial cell layers of the seed coat observed in HT seeds suggests that increased tension was exerted between adjacent cells and that the seed coat cells resisted the tension by cell stretching rather than cell division. Such stress-dependent stiffening of seed coat cell walls has been shown in *iku2* mutants (Creff *et al.*, 2023). Thus, increased stiffness of the seed coat cell walls would resist strain between seed coat cells to compensate for the pressure exerted by the developing embryo. Tight regulation of these opposing forces governs the wall mechanics required for seed growth. Mechanical support of Topas seeds developed under HT by applying a silicone tube partially rescued SCR, strongly suggesting that the seed coat layers lack the strength to withstand the tension from the pressure exerted by the developing embryo. The exact process by which increased pectin demethylesterification plays a role in the wall mechanics of *Brassica napus* seeds is unclear. Our data suggest two possible mechanisms underlying the heat-induced SCR phenotype. First, exposure of seeds to elevated temperatures leads to changes in the seed coat cell wall, making it more susceptible to rupture under the pressure exerted by the expanding embryo. Second, HT-dependent embryo expansion increases the tension on the seed coat and may promote the observed changes in cell wall composition, similar to what happens in *Arabidopsis*. However, these changes may not be sufficient to prevent SCR due to the intense pressure exerted by the growing embryo.

ACKNOWLEDGEMENTS

764 This work was financially supported by the project TowArds Next GENeration Crops, reg. no.
765 CZ.02.01.01/00/22_008/0004581 of the ERDF Programme Johannes Amos Comenius. We
766 acknowledge the Bioinformatics (supported by the NCLG research infrastructure LM2023067
767 funded by MEYS CR), Cell Imaging (supported by MEYS CR LM2023050 Czech-BioImaging), and
768 Plant Sciences Core Facilities of CEITEC Masaryk University for their support in obtaining the
769 scientific data presented in this paper. This work has benefited from the support of IJPB's
770 Plant Observatory platforms Po-Chem. The IJPB benefits from the support of Saclay Plant
771 Sciences SPS (ANR-17-EUR-0007). This work was also supported by a grant from the French
772 ANR (MECHASEED, ANR-23-CE13-0009) to BL.
773

774 **COMPETING INTERESTS**

775 The authors declare no competing interests.
776

777 **AUTHOR CONTRIBUTIONS**

778 HSR secured the funding. UK and HSR conceived the project, designed the experiments, and
779 interpreted the data. UK performed the seed phenotyping, histology, ABA treatments,
780 transcriptomics, and immunolabelling of the seed coat. IU and JH optimised the protocol for
781 Technovit embedding of oilseed rape seed and prepared the slides for histology. AMM
782 analysed the transcriptomic data. AC and BL performed the immunolabelling of the seed coat.
783 AV performed the cell wall profiling. IP, AP and ON performed the hormonal profiling. UK and
784 HSR drafted the manuscript. All authors have proofed and approved the manuscript.
785

786 **DATA AVAILABILITY**

787 The data generated during the current study are included in this published article (and its
788 Supporting Information file) and are available in the Zenodo repository
789 [https://zenodo.org/doi/10.5281/zenodo.14224074]. The dataset supporting the conclusions
790 of this article is deposited to the NCBI repository (BioProject accession number
791 PRJNA1188476, https://www.ncbi.nlm.nih.gov/bioproject/PRJNA1188476).
792

793 **REFERENCES**

794 **Abu-Jamous B, Kelly S**. **2018**. Clust: automatic extraction of optimal co-expressed gene clusters from
795 gene expression data. *Genome Biology* **19**: 172.

Agnolucci P, De Lipsis V. **2020**. Long-run trend in agricultural yield and climatic factors in Europe. *Climatic Change* **159**: 385–405.

Agnolucci P, Rapti C, Alexander P, De Lipsis V, Holland RA, Eigenbrod F, Ekins P. **2020**. Impacts of rising temperatures and farm management practices on global yields of 18 crops. *Nature Food* **1**: 562–571.

Andrews S. **2010**. FastQC: A Quality Control Tool for High Throughput Sequence Data.

Baud S, Kelemen Z, Thévenin J, Boulard C, Blanchet S, To A, Payre M, Berger N, Effroy-Cuzzi D, Franco-Zorrilla JM, *et al.* 2016. Deciphering the molecular mechanisms underpinning the transcriptional control of gene expression by L-AFL proteins in Arabidopsis seed. *Plant Physiology*: pp.00034.2016.

Benech-Arnold RL, Rodríguez M V. 2018. Pre-harvest Sprouting and Grain Dormancy in Sorghum bicolor: What Have We Learned? *Frontiers in Plant Science* **9**.

Bolger AM, Lohse M, Usadel B. **2014**. Trimmomatic: a flexible trimmer for Illumina sequence data. *Bioinformatics* **30**: 2114–2120.

Bond J, Donaldson L, Hill S, Hitchcock K. **2008**. Safranine fluorescent staining of wood cell walls. *Biotechnic & Histochemistry* **83**: 161–171.

Broad Institute, GitHub Repository. **2018**. Picard Toolkit.

Carrillo-Barral N, Rodríguez-Gacio M del C, Matilla AJ. **2020**. Delay of Germination-1 (DOG1): A Key to Understanding Seed Dormancy. *Plants* **9**: 480.

Chu J, Sadeghi S, Raymond A, Jackman SD, Nip KM, Mar R, Mohamadi H, Butterfield YS, Robertson AG, Birol I. **2014**. BioBloom tools: fast, accurate and memory-efficient host species sequence screening using bloom filters. *Bioinformatics* **30**: 3402–3404.

Cosgrove DJ. **2024**. Structure and growth of plant cell walls. *Nature Reviews Molecular Cell Biology* **25**: 340–358.

Creff A, Ali O, Bied C, Bayle V, Ingram G, Landrein B. **2023**. Evidence that endosperm turgor pressure both promotes and restricts seed growth and size. *Nature Communications* **14**.

Creff A, Brocard L, Ingram G. **2015**. A mechanically sensitive cell layer regulates the physical properties of the Arabidopsis seed coat. *Nature Communications* **6**.

Dobin A, Davis CA, Schlesinger F, Drenkow J, Zaleski C, Jha S, Batut P, Chaisson M, Gingeras TR. **2013**. STAR: ultrafast universal RNA-seq aligner. *Bioinformatics* **29**: 15–21.

Ewels P, Magnusson M, Lundin S, Käller M. **2016**. MultiQC: summarize analysis results for multiple tools and samples in a single report. *Bioinformatics* **32**: 3047–3048.

Finkelstein RR, Gampala SSL, Rock CD. **2002**. Abscisic Acid Signaling in Seeds and Seedlings. *The Plant Cell* **14**: S15–S45.

Heino M, Kinnunen P, Anderson W, Ray DK, Puma MJ, Varis O, Siebert S, Kummu M. **2023**. Increased probability of hot and dry weather extremes during the growing season threatens global crop yields. *Scientific Reports* **13**: 3583.

Holdsworth MJ, Bentsink L, Soppe WJJ. **2008**. Molecular networks regulating Arabidopsis seed maturation, after-ripening, dormancy and germination. *New Phytologist* **179**: 33–54.

Jägermeyr J, Müller C, Ruane AC, Elliott J, Balkovic J, Castillo O, Faye B, Foster I, Folberth C, Franke JA, *et al.* 2021. Climate impacts on global agriculture emerge earlier in new generation of climate and crop models. *Nature Food* **2**: 873–885.

Jiang Y, Deyholos MK. **2010**. Transcriptome analysis of secondary-wall-enriched seed coat tissues of canola (Brassica napus L.). *Plant Cell Reports* **29**: 327–342.

Kassambara A. **2018**. 'ggpubr:"ggplot2" based publication ready plots.' R package version 0.17.

Kim W, Lee Y, Park J, Lee N, Choi G. **2013**. HONSU, a Protein Phosphatase 2C, Regulates Seed Dormancy by Inhibiting ABA Signaling in Arabidopsis. *Plant and Cell Physiology* **54**: 555–572.

Kolde R. **2015**. Package 'pheatmap'. R Package 1.7 .

Leprince O, Pellizzaro A, Berriri S, Buitink J. **2016**. Late seed maturation: drying without dying. *Journal of Experimental Botany*: erw363.

Li N, Xu R, Li Y. **2019**. Molecular Networks of Seed Size Control in Plants. *Annual Review of Plant Biology* **70**: 435–463.

Liao Y, Smyth GK, Shi W. **2014**. featureCounts: an efficient general purpose program for assigning sequence reads to genomic features. *Bioinformatics* **30**: 923–930.

Lima RB, Pankaj R, Ehlert ST, Finger P, Fröhlich A, Bayle V, Landrein B, Sampathkumar A, Figueiredo DD. **2024**. Seed coat-derived brassinosteroid signaling regulates endosperm development. *Nature Communications* **15**: 9352.

Liu X, Zhang H, Zhao Y, Feng Z, Li Q, Yang H-Q, Luan S, Li J, He Z-H. **2013**. Auxin controls seed dormancy through stimulation of abscisic acid signaling by inducing ARF-mediated *ABI3* activation in *Arabidopsis*. *Proceedings of the National Academy of Sciences* **110**: 15485–15490.

Love MI, Huber W, Anders S. **2014**. Moderated estimation of fold change and dispersion for RNA-seq data with DESeq2. *Genome Biology* **15**: 550.

Lu W, Tang X, Huo Y, Xu R, Qi S, Huang J, Zheng C, Wu C. **2012**. Identification and characterization of fructose 1,6-bisphosphate aldolase genes in Arabidopsis reveal a gene family with diverse responses to abiotic stresses. *Gene* **503**: 65–74.

Mácová K, Prabhullachandran U, Štefková M, Spyroglou I, Pěnčík A, Endlová L, Novák O, Robert HS. **2022**. Long-Term High-Temperature Stress Impacts on Embryo and Seed Development in Brassica napus. *Frontiers in Plant Science* **13**.

Marin-Rodriguez MC. **2002**. Pectate lyases, cell wall degradation and fruit softening. *Journal of Experimental Botany* **53**: 2115–2119.

Mendu V, Griffiths JS, Persson S, Stork J, Downie AB, Voiniciuc C, Haughn GW, DeBolt S. **2011**. Subfunctionalization of Cellulose Synthases in Seed Coat Epidermal Cells Mediates Secondary Radial Wall Synthesis and Mucilage Attachment . *Plant Physiology* **157**: 441–453.

Mohnen D. **2008**. Pectin structure and biosynthesis. *Current Opinion in Plant Biology* **11**: 266–277.

870 **Nagayama T, Nakamura A, Yamaji N, Satoh S, Furukawa J, Iwai H**. **2019**. Changes in the Distribution
871 of Pectin in Root Border Cells Under Aluminum Stress. *Frontiers in Plant Science* **10**.

872 **National Aeronautics and Space Administration**. **2024**. Global temperature. *Goddard Institute for*
873 *Space Studies*.

874 **Oh E, Yamaguchi S, Hu J, Yusuke J, Jung B, Paik I, Lee H-S, Sun T, Kamiya Y, Choi G**. **2007**. PIL5, a
875 Phytochrome-Interacting bHLH Protein, Regulates Gibberellin Responsiveness by Binding Directly to
876 the *GAI* and *RGA* Promoters in *Arabidopsis* Seeds. *The Plant Cell* **19**: 1192–1208.

877 **Okonechnikov K, Conesa A, García-Alcalde F**. **2016**. Qualimap 2: advanced multi-sample quality
878 control for high-throughput sequencing data. *Bioinformatics* **32**: 292–294.

879 **Park K-C, Kwon S-J, Kim N-S**. **2010**. Intron loss mediated structural dynamics and functional
880 differentiation of the polygalacturonase gene family in land plants. *Genes & Genomics* **32**: 570–577.

881 **Peaucelle A, Braybrook SA, Le Guillou L, Bron E, Kuhlemeier C, Höfte H**. **2011**. Pectin-Induced
882 Changes in Cell Wall Mechanics Underlie Organ Initiation in Arabidopsis. *Current Biology* **21**: 1720–
883 1726.

884 **Pěnčík A, Casanova-Sáez R, Pilařová V, Žukauskaitė A, Pinto R, Micol JL, Ljung K, Novák O**. **2018**.
885 Ultra-rapid auxin metabolite profiling for high-throughput mutant screening in Arabidopsis. *Journal*
886 *of Experimental Botany* **69**: 2569–2579.

887 **Rae GM, David K, Wood M**. **2013**. The Dormancy Marker DRM1/ARP Associated with Dormancy but
888 a Broader Role In Planta. *Developmental Biology Journal* **2013**: 1–12.

889 **Rolletschek H, Muszynska A, Borisjuk L**. **2021**. The process of seed maturation is influenced by
890 mechanical constraints. *New Phytologist* **229**: 19–23.

891 **Rolletschek H, Muszynska A, Schwender J, Radchuk V, Heinemann B, Hilo A, Plutenko I, Keil P,**
892 **Ortleb S, Wagner S, *et al.* 2024**. Mechanical forces orchestrate the metabolism of the developing
893 oilseed rape embryo. *New Phytologist* **244**: 1328–1344.

894 **Safran J, Tabi W, Ung V, Lemaire A, Habrylo O, Bouckaert J, Rouffle M, Voxeur A, Pongrac P,**
895 **Bassard S, *et al.* 2023**. Plant polygalacturonase structures specify enzyme dynamics and
896 processivities to fine-tune cell wall pectins. *The Plant Cell* **35**: 3073–3091.

897 **Secchi MA, Fernandez JA, Stamm MJ, Durrett T, Prasad PVV, Messina CD, Ciampitti IA**. **2023**.
898 Effects of heat and drought on canola (Brassica napus L.) yield, oil, and protein: A meta-analysis.
899 *Field Crops Research* **293**: 108848.

900 **Sechet J, Marion-Poll A, North HM**. **2018**. Emerging Functions for Cell Wall Polysaccharides
901 Accumulated during Eudicot Seed Development. *Plants* **7**: 81.

902 **Šimura J, Antoniadi I, Široká J, Tarkowská D, Strnad M, Ljung K, Novák O**. **2018**. Plant
903 Hormonomics: Multiple Phytohormone Profiling by Targeted Metabolomics. *Plant Physiology* **177**:
904 476–489.

905 **Tai L, Wang HJ, Xu XJ, Sun WH, Ju L, Liu WT, Li WQ, Sun J, Chen KM**. **2021**. Pre-harvest sprouting in
906 cereals: Genetic and biochemical mechanisms. *Journal of Experimental Botany* **72**: 2857–2876.

907 **Turbant A, Fournet F, Lequart M, Zabijak L, Pageau K, Bouton S, Van Wuytswinkel O**. **2016**. PME58
908 plays a role in pectin distribution during seed coat mucilage extrusion through homogalacturonan
909 modification. *Journal of Experimental Botany* **67**: 2177–2190.

910 **Vaistij FE, Gan Y, Penfield S, Gilday AD, Dave A, He Z, Josse E-M, Choi G, Halliday KJ, Graham IA**.
911 **2013**. Differential control of seed primary dormancy in *Arabidopsis* ecotypes by the transcription
912 factor SPATULA. *Proceedings of the National Academy of Sciences* **110**: 10866–10871.

913 **Voxeur A, Habrylo O, Guénin S, Miart F, Soulié M-C, Rihouey C, Pau-Roblot C, Domon J-M,**
914 **Gutierrez L, Pelloux J, *et al.* 2019**. Oligogalacturonide production upon *Arabidopsis thaliana* –
915 *Botrytis cinerea* interaction. *Proceedings of the National Academy of Sciences* **116**: 19743–19752.

916 **Wang L, Wang S, Li W**. **2012**. RSeQC: quality control of RNA-seq experiments. *Bioinformatics* **28**:
917 2184–2185.

918 **Wickham H**. **2011**. ggplot2. *WIREs Computational Statistics* **3**: 180–185.

919 **Wormit A, Usadel B**. **2018**. The Multifaceted Role of Pectin Methylesterase Inhibitors (PMEIs).
920 *International Journal of Molecular Sciences* **19**: 2878.

921 **Wu H-C, Bulgakov VP, Jinn T-L**. **2018**. Pectin Methylesterases: Cell Wall Remodeling Proteins Are
922 Required for Plant Response to Heat Stress. *Frontiers in Plant Science* **9**: 1612.

923 **Wu W, Cao S, Shi L, Chen W, Yin X, Yang Z**. **2023**. Abscisic acid biosynthesis, metabolism and
924 signaling in ripening fruit. *Frontiers in Plant Science* **14**: 1279031.

925 **Xiang Y, Nakabayashi K, Ding J, He F, Bentsink L, Soppe WJJ**. **2014**. REDUCED DORMANCY5 Encodes
926 a Protein Phosphatase 2C That Is Required for Seed Dormancy in *Arabidopsis*. *The Plant Cell* **26**:
927 4362–4375.

928 **Xu Z, Yang M, Li Z, Xiao J, Yang X, Wang H, Wang X**. **2022**. Tissue-specific pectin methylesterification
929 and pectin methylesterase activities play a role in lettuce seed germination. *Scientia Horticulturae*
930 **301**: 111134.

931 **Yamagishi K, Tatematsu K, Yano R, Preston J, Kitamura S, Takahashi H, McCourt P, Kamiya Y,**
932 **Nambara E**. **2009**. CHOTTO1, a Double AP2 Domain Protein of Arabidopsis thaliana, Regulates
933 Germination and Seedling Growth Under Excess Supply of Glucose and Nitrate. *Plant and Cell*
934 *Physiology* **50**: 330–340.

935 **Yano R, Kanno Y, Jikumaru Y, Nakabayashi K, Kamiya Y, Nambara E**. **2009**. CHOTTO1, a Putative
936 Double APETALA2 Repeat Transcription Factor, Is Involved in Abscisic Acid-Mediated Repression of
937 Gibberellin Biosynthesis during Seed Germination in Arabidopsis . *Plant Physiology* **151**: 641–654.

938 **Young LW, Wilen RW, Bonham-Smith PC**. **2004**. High temperature stress of Brassica napus during
939 flowering reduces micro- and megagametophyte fertility, induces fruit abortion, and disrupts seed
940 production. *Journal of Experimental Botany* **55**: 485–495.

941 **Zhao C, Liu B, Piao S, Wang X, Lobell DB, Huang Y, Huang M, Yao Y, Bassu S, Ciais P, *et al.* 2017**.
942 Temperature increase reduces global yields of major crops in four independent estimates.
943 *Proceedings of the National Academy of Sciences of the United States of America* **114**: 9326–9331.

944

945

946 **FIGURE LEGENDS**

947 **Fig. 1.** SCR phenotype observed in Topas seeds developed under HT. (a, b) 26 DAP seeds (a)
948 and their isolated embryos (b) grown under CT. (c, d) 26 DAP seeds (c) and their isolated
949 embryos (d) grown under HT. SCR was observed (*, Δ, +, ●). * Indicates seeds with testa
950 rupture with intact embryo, Δ indicates testa rupture with radicle protrusion, + indicates testa
951 rupture with cotyledon protrusion, and ● indicates embryos with abnormal development. (e)
952 Quantification of the number of dry seeds per silique from CT (blue) and HT (red) showing the
953 number of total, viable, SCR and dead seeds. Asterisks indicate statistically significant
954 differences in HT in a multiple t-test using the Holm-Sidak method (**** corresponds to *p*-
955 values of $p < 0.0001$. (f) Embryo stage of seeds developed on CT (top) and HT (bottom) from
956 14 to 20 DAP. The isolated embryo shown on the right is from the seed on the left. Scale bars:
957 2 mm (a-d) and 3mm (f).

958

959 **Fig. 2.** ABA levels and expression of genes involved in ABA metabolism in *Brassica napus* Topas
960 seeds. (a) Seeds were from 14 DAP to 36 DAP of CT (blue) and HT (red, dark red). From 20
961 DAP, HT seeds were separated into intact seeds (red) and SCR seeds (dark red). Quantification
962 is presented as pmol per g fresh weight. (b) Measurements were performed for ABA, 7-
963 hydroxy-ABA, phaseic acid (PA), and dihydrophaseic acid (DPA) from embryos and seed coats
964 from 14 DAP and 18 DAP seeds grown in CT (blue) and HT (red). Asterisks indicate statistically
965 significant differences in HT and between 14 DAP HT and 18 DAP CT in a multiple t-test using
966 the Holm-Sidak method (*, **, *** and **** correspond to *p*-values of $0.05 > p > 0.01$, $0.01
967 > p > 0.001$, $0.001 > p > 0.0001$ and $p < 0.0001$, respectively); n.s., not significant. (c) 15 siliques
968 of 14 DAP and 18 DAP from HT and CT, respectively, were cultured in the presence or absence
969 of 10 µM ABA (Fig. S1). Dry seeds were quantified for the number of total viable, SCR and
970 dead seeds per silique. Samples with the same letter were not statistically significantly
971 different. (d) Relative expression of selected genes representing DORMANCY ASSOCIATED
972 gene 1 (DRM1) and FRUCTOSE 1,6-BIPHOSPHATE ALDOLASE 6 (FBA6) in 14 DAP (blue), 20 DAP
973 intact (yellow) and 20 DAP SCR (grey) seeds. Data were extracted from the transcriptome
974 dataset (Tables S1 and S2). (e) Heatmap showing the differential expression of selected genes
975 involved in ABA metabolism in 14 DAP, 20 DAP intact, and 20 DAP SCR seeds. The full dataset
976 is provided in Tables S1 and S2.

977

978 **Fig 3.** Embryo and seed size measurements of *Brassica napus* Westar and Topas seeds
979 developed at CT and HT. (a, b) Seed (a) and embryo (b) area measurements in mm^2 of 14, 18
980 and 20 DAP Topas seeds developed at CT (blue) and HT (red). (c, d) Seed (c) and embryo (d)
981 area measurements in mm^2 of 14, 18 and 20 DAP Westar seeds developed at CT (blue) and
982 HT (red). Asterisks indicate statistically significant differences in HT and between 14 DAP HT
983 and 18 DAP CT in a two-way ANOVA test with Sidak's multiple comparisons (*, **, *** and
984 **** correspond to p-values of $0.05 > p > 0.005$, $0.005 > p > 0.0005$, $0.0005 > p > 0.0005$ and
985 $p < 0.00005$, respectively); n.s., not significant. (e) Embryo-to-seed size ratio in 14, 18 and 20
986 DAP Topas and Westar seeds developed at CT and HT. Samples with the same letter were not
987 statistically significantly different. Representative pictures of the seeds and embryos are
988 shown in Fig. S3.
989
990 **Fig. 4** The thickness of the seed coat cells is reduced in HT. (a-e) Histological sections of Topas
991 seeds focused on the seed coat, stained with toluidine blue. (a) The seed coat is composed of
992 an epidermal layer, a palisade layer and an endodermal layer. (b-e) Seed coat of 14 DAP seeds
993 from CT (b) and HT (d) and 18 DAP seeds from CT (c) and HT (e). Scale bars represent 200 µm.
994 (f-h) Box-whisker plots show the size mean, median, outliers, and SD in µm of the thickness
995 of the epidermal layer (f), palisade layer (g) and first endothelial cell layer (h) in 10, 14, 18,
996 and 20 DAP seeds from CT (blue) and HT (red). Samples with the same letter were not
997 statistically significantly different. (i) Percentage of reduction in thickness as the seed aged
998 from 14 to 20 DAP.
999
1000 **Fig. 5** Transcriptional changes in Topas seeds associated with growth at HT indicate changes
1001 in cell wall composition. (a) Principal component analysis using gene expression data from the
1002 samples tested for differences between samples and biological replicates. (b) Heatmap
1003 showing differential transcription of selected genes involved in seed dormancy in 14 DAP, 18
1004 DAP, 20 DAP intact and 20 DAP SCR seeds. Expression in 14 DAP HT seeds is compared with
1005 expression in 18 DAP CT seeds. (c) GO terms related to cell wall associated with the
1006 transcriptional response of Topas seeds to HT are shown. (d) Heatmap showing the
1007 differential transcription of selected genes involved in pectin metabolism in 14 and 18 DAP
1008 seeds grown at CT and HT. The expression in 14 DAP HT seeds is compared with the expression
1009 in 18 DAP CT seeds. The full dataset is presented in Tables S1, S2 and S3.

1010

1011 **Fig. 6** The composition and properties of the seed coat cell wall are altered in HT-grown seeds.
1012 (a, b) Histological sections of Topas seeds focused on the seed coat, stained with Ruthenium
1013 Red for pectin (a) and Safranin-O for lignin (b). Sections of 14, 18, and 22 DAP CT seeds and
1014 14 and 18 DAP HT seeds are shown. Scale bars represent 200 µm. (d-g) Immunolocalization
1015 of pectin and xyloglucans using LM19, JIM5, LM20 and LM25 antibodies on the testa of 14
1016 and 18 DAP HT and CT seeds. The signal is visible in green, the cell structure is marked in
1017 magenta with calcofluor white. Scale bars represent 100 µm. Fluorescence intensity was
1018 measured in epidermal and palisade cells in 10, 14 and 18 DAP HT and CT seeds. Asterisks
1019 indicate statistically significant differences in HT and between seed ages in a one-way ANOVA
1020 test with Tukey multiple comparisons (*, **, *** and **** correspond to *p*-values of $0.05 > p$
1021 > 0.01, $0.01 > p > 0.001$, $0.001 > p > 0.0001$ and $p < 0.0001$, respectively); n.s., not significant.
1022 (h) Pectin composition of the seed coat cell wall of 10, 14, and 18 DAP seeds from HT and CT.
1023 The graph shows the measurements expressed as peak area from the MS analysis for GalA3,
1024 GalA3ox, GalA3Xyl, GalA3Me, GalA3MeAc, GalA4Ac, GalA4Me, GalA4Meox, GalA4Me-H_2O
1025 and DPx>4Mey (methylesterified OGs with degree of polymerisation greater than 4). (i) Graph
1026 showing the total intensity signal for pectin from (d-f). (j) Graph showing the amount grouped
1027 as methylesterified versus non-methylesterified OGs from (h). (k) Graph showing the
1028 measurements presented as peak area from the MS analysis for xyloglucans. (l) Graph
1029 showing the total intensity signal for xyloglucan from (g). Samples with the same letter were
1030 not statistically significantly different. (m) A 3-mm silicon tube was applied to siliques from 10
1031 DAP CT and 12 DAP HT. Dry seeds were quantified for the number of total viable, SCR and
1032 dead seeds per silique. Asterisks indicate statistically significant differences in HT and
1033 between seed ages in a two-way ANOVA test with Tukey multiple comparisons (*, **, *** and
1034 **** correspond to *p*-values of $0.05 > p > 0.01$, $0.01 > p > 0.001$, and $p < 0.001$, respectively);
1035 n.s., not significant.

1036

1037

1038 **SUPPORTING INFORMATION**

1039 Additional Supporting Information may be found online in the Supporting Information section
1040 at the end of the article.

1041 **Fig. S1** Representative picture of the silique culture system for ABA treatment.

1042 **Fig. S2** Profiles of auxin and its metabolites in *Brassica napus* Topas seeds, isolated embryos
1043 and seed coats.
1044 **Fig. S3** Representative pictures of the seeds and embryos measured in Fig. 3.
1045 **Fig. S4** Venn diagrams summarising the transcriptional response of Topas seeds to HT.
1046 **Fig. S5** GO terms associated with the transcriptional response of Topas seeds to HT.
1047 **Fig. S6** Expression clusters of the transcriptional response of Topas seeds to HT.
1048 **Table S1** Full dataset for the DEGs for all the comparisons.
1049 **Table S2** DEGs for dormancy, ABA and pectin metabolism related.
1050 **Table S3** Misregulated GO terms associated with plant cell wall, hormone, cell cycle,
1051 metabolic, heat response and developmental pathways.
1052 **Table S3** DEGs and GO terms associated with each of the clusters.
1053 **Methods S1** Co-expression cluster mapping of genes.